

LANDSLIDE RISK  
SCREENING  
USING REMOTE  
SENSING  
**SOUTH ASIA**

Public Disclosure Authorized

Public Disclosure Authorized

Public Disclosure Authorized

Public Disclosure Authorized



EUROPEAN UNION



**GFDRR**  
Global Facility for Disaster Reduction and Recovery



Administered by  
**THE WORLD BANK**  
IBRD • IDA | WORLD BANK GROUP

---

This work is a product of the staff of The World Bank and the Global Facility for Disaster Reduction and Recovery (GFDRR) with external contributions. The findings, analysis and conclusions expressed in this document do not necessarily reflect the views of any individual partner organization of The World Bank, its Board of Directors, or the governments they represent.

Although the World Bank and GFDRR make reasonable efforts to ensure all the information presented in this document is correct, its accuracy and integrity cannot be guaranteed. Use of any data or information from this document is at the user's own risk and under no circumstances shall the World Bank, GFDRR or any of its partners be liable for any loss, damage, liability or expense incurred or suffered which is claimed to result from reliance on the data contained in this document. The boundaries, colors, denomination, and other information shown in any map in this work do not imply any judgment on the part of The World Bank concerning the legal status of any territory or the endorsement or acceptance of such boundaries.

#### RIGHTS AND PERMISSIONS

The material in this work is subject to copyright. Because The World Bank encourages dissemination of its knowledge, this work may be reproduced, in whole or in part, for noncommercial purposes as long as full attribution to this work is given.

The cover image: Photo by Masatsugu Takamatsu

Image Detail: A road blockage due to a landslide in Nepal

---

# CONTENTS

---

<b>ACKNOWLEDGMENTS</b>	<b>4</b>	<b>6. <i>IN SITU</i> MONITORING AND VALIDATION</b>	<b>38</b>
<b>ABBREVIATIONS</b>	<b>5</b>	6.1 Introduction	38
<b>1. EXECUTIVE SUMMARY</b>	<b>6</b>	6.2 Method of Site Selection and Slope Monitoring	38
<b>2. INTRODUCTION</b>	<b>8</b>	6.2.1 Selection of the Pilot Sites	38
2.1 Project Objectives	9	6.2.2 Building a Slope Monitoring System	40
<b>3. STUDY SITES</b>	<b>10</b>	6.3 Result and Discussion	42
3.1 Site 1: Road near Rudraprayag, India	10	6.4 Summary and Future Plan	44
3.2. Site 2: Road near Reotala, Bhutan	11	<b>7. DATA PRESENTATION AND SHARING PLATFORMS</b>	<b>45</b>
3.3. Site 3: Along the Rapti Highway (Road H11 near Sharada) Nepal	11	7.1 GIS Files: ESRI Shapefiles and Google Earth .kmz Files	45
<b>4. METHODS</b>	<b>12</b>	7.2 ArcGIS Online Webmaps	45
4.1 Satellite-Based Radar Displacement Monitoring	12	<b>8. GENERAL DISCUSSION AND CONCLUSIONS</b>	<b>46</b>
4.2 PS Points: Filtering and Clustering	14	8.1 PS InSAR Data Generation and Interpretation within the Context of Slope Stability and Landslides	46
4.3 Hazard Scoring	18	8.2 Translating InSAR Displacement and Velocities into a Measure of Hazard and Combining It with Exposure Information to Provide a First-Order Risk Estimation	47
4.4 Exposure Scoring	19	8.3 System Setup and Workflow	48
4.5 Risk Priority Rankings	19	8.4 Benefits of InSAR and <i>In situ</i> -Based Slope Monitoring	49
<b>5. DETAILED ANALYSIS OF KEY LANDSLIDE LOCATIONS</b>	<b>20</b>	8.5 Challenges and Lessons	49
5.1 Results for Site 2: Road near Reotala, Bhutan	20	8.6 Future Opportunities	50
5.1.1 PSI Processing	21	<b>REFERENCES</b>	<b>54</b>
5.1.2 PS Points: Filtering, Clustering, and Displacement Time Series	22	<b>APPENDIX</b>	<b>56</b>
5.1.3 Hazard, Exposure, and Risk Rankings	24		
5.1.4 Relationship with Possible Landslide Areas	28		
5.2 Results for Site 1: Road near Rudraprayag, India	30		
5.2.1 PSI Processing	30		
5.2.2 PS Points: Filtering, Clustering, and Displacement Time Series	30		
5.2.3 Hazard, Exposure, and Risk Rankings	32		
5.3 Results for Site 3: Along the Rapti Highway (Road H11 near Sharada) Nepal	34		
5.3.1 PSI Processing	34		
5.3.2 PS Points: Filtering, Clustering, and Displacement Time Series	34		
5.3.3 Hazard, Exposure, and Risk Rankings	36		

---

## ACKNOWLEDGMENTS

---

Production of the report was led by **Masatsugu Takamatsu**, Disaster Risk Management (DRM) Specialist in South Asia Region Climate Change and Disaster Risk Management (SSACD). The report was prepared by **Professor Thomas Oommen** (Technical Leader), **Dr. Rudiger Escobar Wolf**, and **El Hachemi Bouali** from the Department of Geological & Mining Engineering & Science, Michigan Technological University. The field investigation part, summarizing the contents of Japan International Cooperation Agency (JICA) Technical Cooperation Project, of the report was prepared by **Ryota Hasegawa**, **Tomoharu Iwasaki** and **Takeshi Kuwano** from Kokusai Kogyo Co., Ltd. The team extends sincere appreciation to the following World Bank peer reviewers for insightful and useful comments: **Elif Ayhan** (Senior DRM specialist), **Henrike Brecht** (Senior DRM Specialist), **Ocean Keau** (Transport Specialist), **Fiona Collin** (Lead Transport Specialist), **Priyanka Dissanayake** (DRM Specialist), **Nagaraja Rao Harshadeep** (Lead Environment Specialist), and **Michael Norton** (Consultant). The report greatly benefited from professional editorial work by **Hope Steele**, **Mehsum Basharat**, and professional graphic design by **Errica Mallozzi**. The team would like to extend sincere appreciation to the Department of Roads in Bhutan, Department of Roads in Nepal, and Department of Public Works in Uttarakhand for providing useful information and inputs to the study. Special acknowledgments go to the following World Bank staff: **Keisuke Iyadomi**, **Hemang Karelia**, **Erika Vargas**, **Christoph Pusch**, **Henriette Mampuya**, **Dechen Tshering** (Consultant), **Avani Mani Dixit**, **Deepak Man Singh Shrestha**, and **Sachi Suzuki**.

Finally, the team would like to appreciate support from **Abhas Jha**, Practice Manager of SSACD, and **Niels Holm-Nielsen**, Practice Manager of the Global Facility for Disaster Reduction and Recovery (GFDRR). This analytical work was conducted under the trust fund project *Building Resilience to Landslide and Geohazard Risk in the South Asia Region* in the frame of the South Asia Capacity Building for Disaster Risk Management Program funded by the European Union. The Task Team would like to express sincere appreciation to the European Union for its generous financial support to this work.

This technical report contents are sole responsibility of the Task Team. The European Union is not responsible for any use that may be made of the information contained therein.

---

## ABBREVIATIONS

---

DEM	digital elevation model
DoR	Department of Roads
ESA	European Space Agency
InSAR	interferometric synthetic aperture radar
JICA	Japan International Cooperation Agency
PNH1	Primary National Highway No. 1
PNH4	Primary National Highway No. 4
PS	persistent scatterers
PSI	persistent scatterer interferometry
SAR	synthetic aperture radar
SLC	Single Look Complex
SRTM	Shuttle Radar Topography Mission
WB	World Bank

## EXECUTIVE SUMMARY

01

Image:

A road blockage due to a landslide in Nepal  
(Photo by Masatsugu Takamatsu)

Landslides pose a significant risk for development in South Asia, the home of the Hindu Kush and Himalayan mountains. Out of all the landslides that occur across the globe, around 60% occur in South Asia. Sustainable development needs ways to identify, monitor, and mitigate landslide hazards. The traditional methods to monitor landslides with onsite equipment are costly and prohibitive for large-scale infrastructure projects.

Remote sensing using satellite and aerial platforms provides an alternative to deliver a broad assessment of a vast region and quantitative measurements. The technology is useful, especially in a region such as the Himalayas, where the terrain is very hilly and difficult to access for field inspection. In this World Bank Project (hereafter, the WB Project), we applied a type of remote sensing analysis called satellite-based interferometric synthetic aperture radar (InSAR) for landslide monitoring in parts of India, Bhutan, and Nepal. The study areas in India, Bhutan, and Nepal were 1,404 square kilometers, 379 square kilometers, and 268 square kilometers, respectively.

We used images taken by Sentinel-1 satellite and applied an analysis called persistent scatterer interferometry (PSI). First, the analysis provides a large number of persistent scatters that could

be used to measure ground displacement. Second, we filtered out less important points (i.e., small displacements or low coherence) and focused on high priority points where the changes were happening fast with high confidence. Third, the filtered points were clustered based on the velocity and proximity of points. The clustering enabled us to find a group of points that showed the same behavior and further refine our attention to critical locations having large displacement in the region. Fourth, by plotting the displacement time series of these clusters, we visualize the pace of ground movement over time at different clusters. We observed some clusters show constant fast movements, which could eventually cause massive displacements and failure. To identify high-risk clusters, we used the displacement information obtained from the analysis and combined with slope information based on elevation data to give hazard weighting. Lastly, this hazard weighting was combined with an exposure rating, which considered the presence of houses and roads nearby that would be destroyed in the case of a failure. The combination of hazard weighting and the exposure rating helped us to figure out which clusters needed the most attention. The critical locations identified are near Rudraprayag in India, Reotala Bridge in Bhutan, and in Sharada along the Rapti Highway in Nepal. The analytical process applied in this report is visualized below.

## METHODS

### STUDY AREAS in square kilometers

1,404

India

379

Bhutan

268

Nepal



PSI  
ANALYSIS  
OF IMAGES

The Sentinel-1 satellite images were used for the study. The PSI analysis of the Sentinel-1 data provided a large number of persistent scatterers (PS) that could be used to measure ground deformation.



FILTER

Subsequent filtering was applied to the PS using high velocity and high coherence as the filtering criteria. The filtering enabled a reduction in the number of points to be analyzed and allowed the analysis to focus on the points of higher priority.

CLUSTER



The filtered point was clustered based on the velocity and coherence of the PS. The clustering enabled the identification of a group of points that indicate uniform behavior and further filter out the individual points that could potentially be influenced by noise.

DISPLACEMENT  
TIME SERIES



Plotting the displacement time series of these datasets showed constant velocity displacements at these sites. Although the fact that these points are not accelerating is good news, it certainly is a concern that these constant velocity movements can, in the long term, lead to massive displacements and failure.

WEIGHTED BY  
VELOCITY &  
SLOPE



The velocity obtained from the InSAR was combined with the slope for the hazard weighting with velocity being weighted as twice as important as the slope.

The percentile of the slope and velocity was used to create three weight classes: > 90th was weighted the highest, followed by 50th-90th, and then < 50th.

WEIGHTED  
HAZARD &  
EXPOSURE RATES



The hazard weighting was combined with an exposure rating, which considered the presence of houses and roads.



FIELD  
INSPECTION

Conduct field inspection or field monitoring of the identified high priority sites



TOTAL RISK  
SCORE RANKED

The combination of hazard weighting and the exposure rating provided the total risk score that enables us to rank the clustered velocities for identifying priority sites.

## RESULTS & FINDINGS

In **Bhutan**, rainfall-induced landslides along the road near Reotala have been recurring for many years and causing frequent and long road closures for repairs. The analysis identified that some clusters were persistently moving with constant speed and prioritized three high risk sites where onsite investigation is recommended. Based on the analysis result, Japan International Cooperation Agency (JICA) selected sites for instrumentation and piloted rainfall threshold-based early warning systems. The system included rain gauges and tilt sensors and was installed at two sites in 2019. The tilt sensor data from the early warning system successfully monitored the precursors and the timings of occurrence of slope failures. The remote sensing-based InSAR work (WB Project) and the early warning system (JICA Project) demonstrates how the Department of Roads (DoR) and other government agencies can utilize these techniques for macro-and micro-scale monitoring of landslide hazard and disaster risk reduction. The report also demonstrates the complementarity of the remote sensing-based and in onsite landslide monitoring techniques in disaster risk reduction.

Similarly, the InSAR analysis was conducted for roads near Rudraprayag in **Uttarakhand, India**, which have a long history of landslides. The area experienced rainfall-triggered landslides in

2012, 2013, and 2014 killed many and disrupted traffic. In **Nepal**, the target site is along the Rapti Highway which stretches about 200 kilometers and crosses variety of landscapes in western part of the country. High slopes and intense or prolonged rainfall have been causing frequent landslides. Recent landslides blocked and damaged the highway. This InSAR analysis identified 10 highest risk scored clusters each in India and Nepal as well.

This study's main findings are that the InSAR method can be valuable to screen large areas for slope movements. Such information can help plan future investments, identify sites for onsite monitoring or further field investigation, and manage risk to infrastructure and communities. When large infrastructure investments such as building a new road are made in the landslide-prone area, traditionally, landslide susceptibility analysis is performed based on spatial information such as topography, soil, land use, etc. to provide info on spatial locations that could potentially fail due to landslides. This can be cross-checked or complemented by the InSAR analysis providing historical or current displacement information. Such information can help agencies make safer investments, prioritize slope stabilization and hazard mitigation efforts, and reduce community risk of landslide hazards.

---

## INTRODUCTION

---

02

Landslide risk represents one of the most severe problems related to natural hazards on a global scale (equivalent to over 4,500 deaths each year), particularly in areas with high relief (Highland and Bobrowsky 2008).

There have been new developments such as the Satellite-based interferometric synthetic aperture radar (InSAR), which measures ground displacement on a millimeter scale and produces time series data of such high-precision measurements by applying image stacking techniques (Bouali, Oommen, and Escobar-Wolf 2016, 2018). Using lessons from applying the InSAR method to landslide-prone areas in India, Bhutan, and Nepal, this report highlights a blueprint of the hazard planning that can be very effective for roads in hilly areas across the region.

Transportation corridors (roads, railroads, etc.) traversing landslide risk-prone regions are particularly exposed to such hazards (Klose, Damm, and Terhorst 2015; Winter et al. 2016). Further, landslides directly endanger people and their livelihoods, directly threatening populated centers as well. Improper design and execution of development projects such as roads in mountainous terrains can increase slope instability and result in landslides. To mitigate the risk from landslides, it is necessary to characterize and monitor the hazard based on sound scientific and technical methodologies—see, for example, Corominas et al. 2014 and references therein for a compilation, as well as Fell et al. 2008 for guidelines on behalf of the JTC-1 Joint Technical Committee on Landslides and Engineered Slopes. There are a plethora of different mapping methodologies that can assess the spatial distribution of the landslide-prone areas, but to plan for hazards in areas that may be exposed to the landslide hazard, it is crucial to monitor how the hazard evolves through time.

Slope instability may progress in a way that could give opportunities to warn of the imminence of collapse, especially when the instability develops over long periods of time and is driven by a steady and relatively slow process. Landslides triggered by external factors that include seismic forces, water infiltration from intense and prolonged rainstorm events, and so on may not show precursory displacement. In some cases, however, the hazard monitoring for such landslides can be included in monitoring the triggering events—for example, in the case of rainfall by tracking storm systems that could pose such a threat. This study focuses on the slopes that depict a long-term behavior which can be used as a precursor to forecast the occurrence of landslides (Highland and Bobrowsky 2008), more specifically the relatively small-scale displacement or movement of the slope. Surface movement potentially indicates two factors: (i) that the slope is becoming unstable and (ii) that a landslide may be likely to happen sometime in the future. Although it is difficult to infer an exact timing from the displacement data, general conclusions about the likelihood of different slopes to fail can be made based on the velocity at which the slope is moving; whether the slope



movement is accelerating, decelerating, or moving at a constant speed; and other slope characteristics (e.g., the slope angle, etc.).

Slope movement can be very subtle, only a few millimeters per year, but this small movement can still be significant in relation to slope stability. Measuring displacements and velocities on such a small scale can be challenging, particularly over extensive areas that may be prone to landslides in rugged terrain. In situ measurement methods, including geodetic and topographic surveying, have the tendency to be very labor-intensive expensive and maybe practical only for limited high-priority areas. A good alternative is remote sensing methods that offer synoptic, large coverage data acquisition and processing capabilities. Satellite-based interferometric synthetic aperture radar (InSAR) provides a very sensitive method of measuring ground displacement at the millimeter scale and produces time series of such high-precision measurements by applying image stacking techniques (Bouali, Oommen, and Escobar-Wolf 2016, 2018). Such methods give information of the deformation at a large number of points (tens to hundreds of thousands) over hundreds of square kilometers and over time periods of several years, with a temporal resolution of only a few days to weeks.

Another shortcoming of the in situ instrumentation is that it can be really challenging when several locations have to be monitored. Besides, in some regions with rugged terrains, the installation and maintenance of in situ instrumentation itself is a difficult task owing to the site's inaccessibility as well as vandalism concerns. In such situations, in situ measurements can be made only at select locations, and remote sensing is the only viable alternative for continuously monitoring critical slopes. This is where synthetic aperture based (SAR)- based remote monitoring of slopes can help collect crucial data. The benefit of using (SAR)-based remote monitoring of the slopes is that the SAR sensors can obtain data during either day or night and are not impacted by cloud cover. The anytime and all-weather data acquisition capabilities of SAR make it a suitable choice for slope stability analysis which can in turn enable and inform policy makers to make timely decisions.

An added benefit for this methodology is that it makes it possible to rank different slopes according to their potential hazard level as inferred from the displacement, velocity, slope angle, and so on in a way that prioritizes which slopes require more attention in a hazard mitigation effort – making it an impactful tool for policy makers. The exact physical interpretation (the cause of slope movement) of the displacement data obtained from remote sensing requires a more in-depth knowledge of the characteristics of the slope in question, which would require collecting field data and samples to characterize that slope. Nevertheless, using just the displacement and velocity data, along with some general characteristics of the slope that can also be obtained from remote sensing (e.g., the slope angle),

Hazard alone is not the only relevant factor to consider

when planning to mitigate risk; it is the risk itself— the actual combination of hazard and vulnerability (or at least exposure)—that is relevant for decision-making about protecting life and avoiding loss. In its most basic form, the vulnerability can be roughly quantified by the exposure of the population, infrastructure, and other valuable assets to the hazard. Using exposure as a proxy for vulnerability may be a valid first-order approximation. In the case of landslides, that typically are intensely destructive phenomena.

This report is an effort to equip hazard planning agencies and policy makers in mitigating the risks associated with landslides. It does so by describing the results of successfully applying the InSAR method to test areas prone to landslides in India, Bhutan, and Nepal. The landslide hazard for multiple sites in the study area was characterized and ranked based on criteria derived from the displacement and velocity data obtained from the InSAR study. The exposures of populations (via identified populated areas) and roads were used as a proxy for vulnerability and were assessed and ranked for each of the considered sites. Hazard and exposure rankings were combined in a single risk ranking for each site in the study area, which allowed prioritizing areas that may be chosen for intervention or risk mitigation efforts. All the ranking methods, including the weights used for each category, were also assigned to make the methodology transparent and allowing the user to provide their inputs and be able to change the weighting values according to their criteria and needs.

In Bhutan, the priority sites identified as part of the WB Project were utilized by Japan International Cooperation Agency (JICA) to select sites for instrumentation to develop rainfall threshold-based early warning systems. The *in-situ* slope monitoring results are also presented in the report as field verification.

## 2.1 PROJECT OBJECTIVES

- Apply InSAR stacking methods to three selected road corridor sites in India, Bhutan, and Nepal, to identify and track slope movements associated with potential slope instabilities and future landslides, over a period of several years, depending on the availability of radar imagery.
- Analyze the slope movement data and interpret them in the context of potential slope instability and land sliding process in both a written report and a set of GIS dataset outputs.

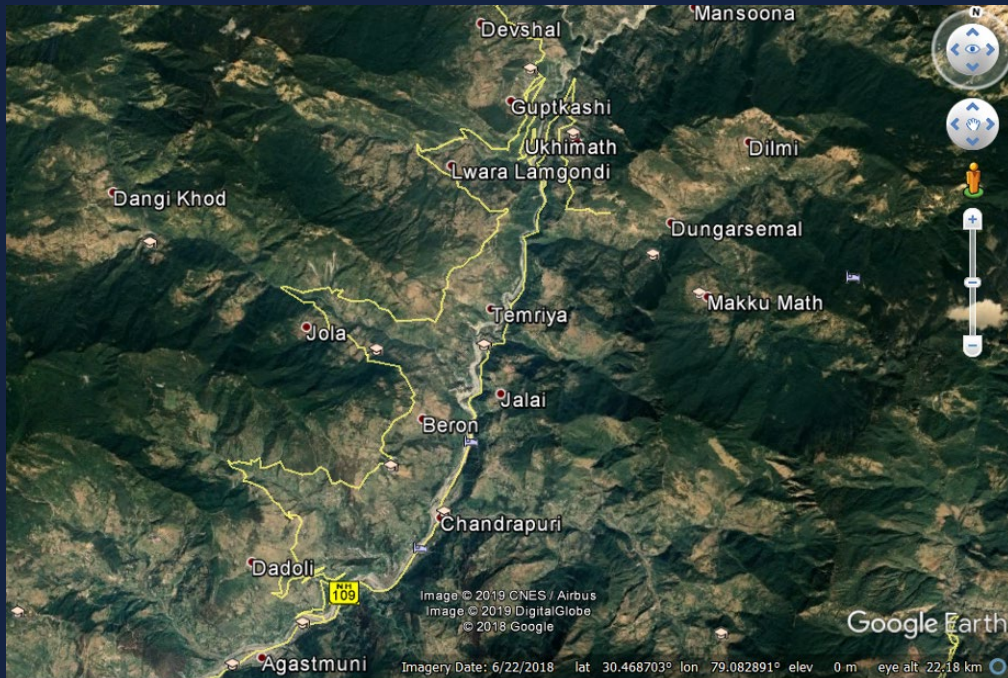


Figure 1.

Google Earth map showing the general outline of site 1, Road near Rudraprayag, India, June 22, 2018

## STUDY SITES

03

THREE SITES WERE SELECTED IN MOUNTAINOUS REGIONS OF INDIA, BHUTAN, AND NEPAL

### 3.1 SITE 1: ROAD NEAR RUDRAPRAYAG, INDIA

The Rudraprayag district in India has a long history of landslide occurrences. Bist and Sah (1999) reported a series of landslides that occurred in August of 1998. The landslides were explained as a consequence of the local geology and relief, but they were triggered by extreme rainfall. Road construction in the area was also recognized as a slope-destabilizing factor. These events left 101 people dead and a large number of houses and infrastructure damaged or destroyed. More recently, the area has also experienced rainfall-triggered landslides: in 2012 (Islam, Chatteraj, and Ray 2014), 2013 (Bhambri et al. 2016), and 2014 (Gupta et al. 2016). The September 2012 landslides caused many deaths, property damage, and road traffic disruption; they were triggered by heavy and prolonged rainfall in an area of landslide-susceptible terrain (weak rocks and soil on steep slopes). The June 2013 events killed a large number of people, and the May 2014 events blocked the Tilwada-Guptkashi route (*Jagran Post* 2014). Landslides triggered by heavy rainfall again blocked a road—this time the Srinagar-Rudraprayag National Highway in June of 2017 (*Times of India* 2017).

Figure 1 shows a Google Earth map of the area of interest. The area is set in a very steep topography related to a north-south trending valley. A series of roads runs parallel to the valley and connects several smaller villages. The river at the bottom of the valley could also be a factor contributing to slope instability if slope undercutting occurred as a consequence of riverbank erosion.



Figure 2.

Google Earth map showing the general outline of site 2, October 18, 2017

### 3.2. SITE 2: ROAD NEAR REOTALA, BHUTAN

Landslides along the road near Reotala have been a recurring problem for many years. Rainfall-induced landslides at the Reotala road have been recurring for many years. In July 2013, several landslides blocked the road (BBS 2013). The Reotala road was again reported to be blocked in September 2015 (BBS 2016; KuenselOnline 2015). The Reotala bridge remained closed for almost five months following damage from landslides in 2016 (KuenselOnline 2016). In July 2017 landslides again blocked the road near Reotala (BBS 2017; KuenselOnline 2017). And as recently as August 4, 2018, the Reotala road had again been blocked by landslides (KuenselOnline 2018).

The road is located on steep, mountainous terrain, close to a river, and potentially subject to the riverbank and slope undercutting due to erosion. The population, or at least the density of villages, in this area seems to be less than in site 1.

Figure 2 shows a Google Earth map of the area identified for site 2. A system of valleys running from southeast to northwest and from southwest to northwest intersect at right angles, resulting in this rugged topography. Main roads run parallel to valley floors not very far from the river contained by these valleys.

### 3.3. SITE 3: ALONG THE RPTI HIGHWAY (ROAD H11 NEAR SHARADA) NEPAL

The Rapti Highway (H11) in Nepal stretches about 200 kilometers and crosses a variety of landscapes, including a long segment located along mountainous and steeply sloped terrain. As with many areas in Nepal, the conjunction of high slopes and intense or prolonged rainfall (Upreti and Dhital 1996) tends to cause frequent landsliding events along the Rapti Highway. In October 2009, landslides disrupted traffic along the Rapti Highway (*The Himalayan Times* 2009). Landslides in October 2013 blocked the Rapti Highway, stranding at least nine vehicles (*Kathmandu Post* 2013). In August of 2014, the highway was again blocked by landslides (*Nepal Monitor* 2014). As recently as August 7, 2018, parts of the road had collapsed as a result of landslides associated with heavy rainfall (*Kathmandu Post* 2018; Reliefweb 2018).

Figure 3 shows a Google Earth map of the general area for site 3. The area is characterized by many smaller valleys cut by a complex network of streams. Although the slopes are not very long, they can still be very steep. The main roads follow river valley bottoms to connect a series of small towns dispersed over the rough topography.

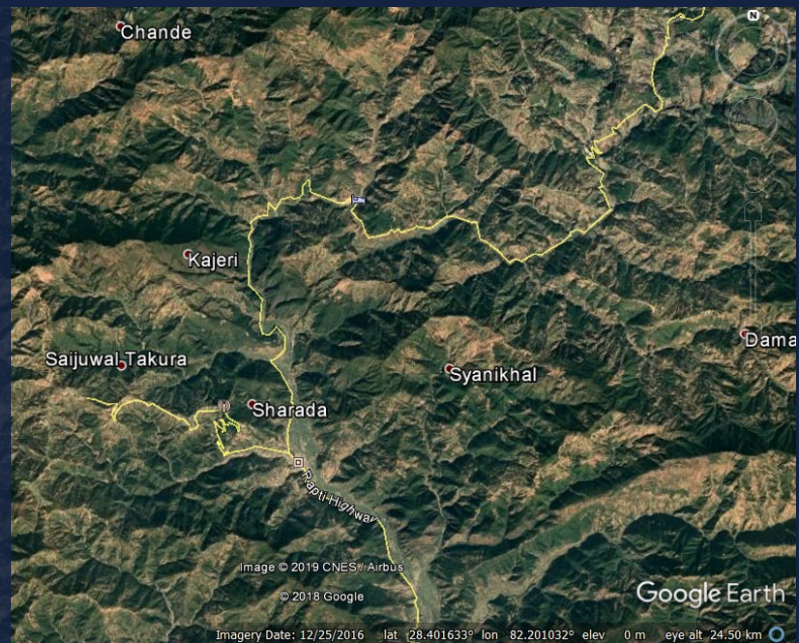


Figure 3.

Google Earth map showing the general outline of site 3, December 25, 2016

## METHODS

04

### 4.1 SATELLITE-BASED RADAR DISPLACEMENT MONITORING

Persistent scatterer interferometry (PSI) is a remote sensing technique that measures geophysical and geometric changes of ground targets using radar image stacks (Ferretti, Prati, and Rocca 2000, 2001). Coherent points, known as *persistent scatterers* (PS), are identified in every image to produce a point cloud, and each PS within the point cloud includes sufficient data to create a displacement-time series. PSI has been widely used for the long-term monitoring of dynamic processes, with many recent studies focusing on landslides (Bianchini et al. 2015; Bouali et al. 2017; Rosi et al. 2018; Xue et al. 2015).

Sentinel-1C SAR antenna captures radar images in the interferometric wide-swath mode. Data relevant to PSI processing are Level-1 Single Look Complex (SLC) products. Images were acquired at a central frequency of 5.405 GHz—the corresponding wavelength of 5.6 centimeters (C-band)—with an incidence angle broadly between 26° and 44.28°, depending on swath and burst numbers, and a spatial resolution of 20 meters across a 250 kilometer swath (see figure 4 for Sentinel-1 operation modes).

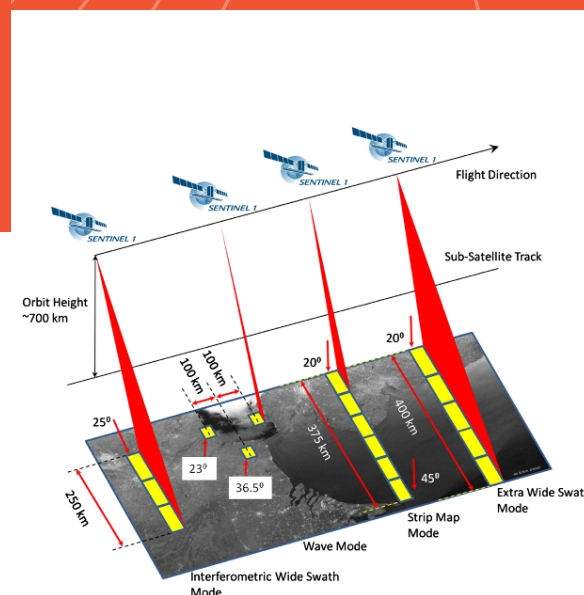


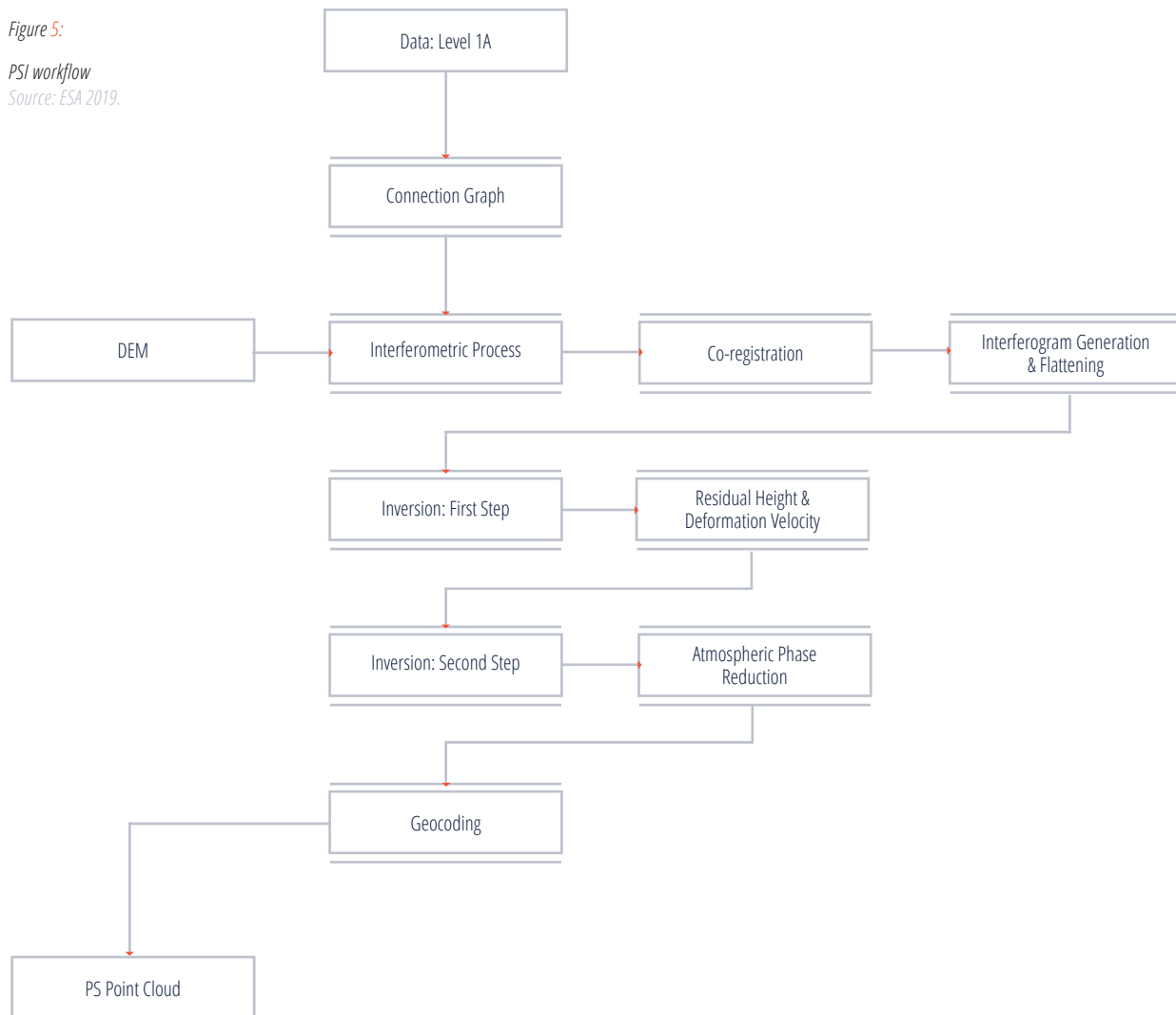
Figure 4:

Sentinel-1 operation modes  
Source: ESA 2019.

Sentinel-1 images are acquired by the European Space Agency (ESA). Images were provided free of charge by the ESA through the Copernicus Open Access Hub. Level-1 SLC products arrive as focused data in slant range, complex form with no Doppler projection, and include the following pre-processing steps (performed by ASI from Level 0 RAW products): gain receiver compensation, internal calibration, data focusing, statistical estimation of the output data, and data formatting into the output.

All Sentinel-1 radar images were processed with the ENVI SARscape PSI software package (Sarmap 2017). ENVI + SARscape PSI Workflow (figure 5) contains five main steps: (1) composing the connection graph; (2) using the interferometric process that comes from the digital elevation model (DEM); (3) performing the first step of the inversion; (4) performing the second step of the inversion; and (5) geocoding the results.

Figure 5:  
PSI workflow  
Source: ESA 2019.



Spatial and temporal baselines were calculated between all image pairs to determine the master image in a time-position plot. Lines connecting the master image to other images in the time-position plot represent interferograms that were generated and flattened after image pairs were co-registered, all of which occurred in the interferometric process step and required a DEM (e.g., 30-meter Shuttle Radar Topography Mission digital elevation model). The first step of the inversion runs the model inversion to derive residual height and deformation velocity used to re-flatten, unwrap, and refine complex interferograms only at locations with coherent radar signal reflectors (coherence threshold = 0.60). The second step of the inversion estimated and removed atmospheric phase components from the model. An atmospheric low-pass filter accounted for the spatial distribution of noise using a two-dimensional moving window (smaller window results in a stronger filter). An atmospheric high-pass filter accounted for temporal distribution of noise using a temporal window

over each area within an image (a shorter window corrects for short-term, drastic atmospheric changes). Geocoding converted phase shift into ground displacement for all PS within each Sentinel-1 radar image relative to the earliest acquisition date. The result is a PS point cloud. Every PS in the point cloud contains the following information: displacement (in millimeters) at each acquisition; average velocity (millimeters/year); coherence; location within a three-dimensional, geocoded coordinate system (x, y, z); line-of-sight incidence angle and azimuth direction of the radar signal; original location within slant range coordinate system (azimuth, range); and precision estimates of height (meters) and velocity (millimeters/year).

## 4.2 PS POINTS: FILTERING AND CLUSTERING

The PS InSAR technique can produce a large number of points (> 1,000,000); the actual number depends on the choice of a coherence threshold. All the points, however, convey the same amount of information, and each point is also affected differently by random noise and the strength of the signal being measured. To identify and isolate only those points that convey the maximum amount of information and to avoid potential noise and artifacts, we selected those points with a high signal-to-noise ratio and a high signal quality. To do this, we use two criteria for our filtering algorithm: the coherence of the PS InSAR processing and the minimum velocity.

The coherence of the PS InSAR processing gives us a measure of how high the correlation is across the set of PS points. In other words, coherence is a measure of data quality. The higher the coherence, the better the displacement and velocity data quality, and the lower the possibility that a PS point is showing noise instead of an actual displacement signal. The second criterion used was the velocity of the PS points. The velocity is derived from the cumulative displacements over time by linear regression of the displacement with respect to time—so the velocity is

equivalent to the slope of the linear regression trend line. A higher velocity can be used as a proxy for a less stable configuration of a slope, although the stability obviously depends on many other variables (e.g., slope inclination, material strength, loads, water pore pressure, etc.). In the next section, we include one more criterion for our hazard estimation (ranking), which is also easy to assess from remote data: the slope angle.

The PS points at site 1 can be used as an example to illustrate the coherence and velocity filtering process.

*Figure 6 shows a map with the original 606,075 PS points processed for site 1.*

*Figure 7 shows the two-dimensional point density map of the two parameters (velocity and coherence) for all the PS points analyzed for site 1. The higher coherences are observed for the lower velocities; this poses a challenge when trying to choose points with both high coherence and high velocity. However, the relatively uniform distribution of velocities means that there will still be enough points at the higher end of the velocity range that also show relatively high coherence values.*

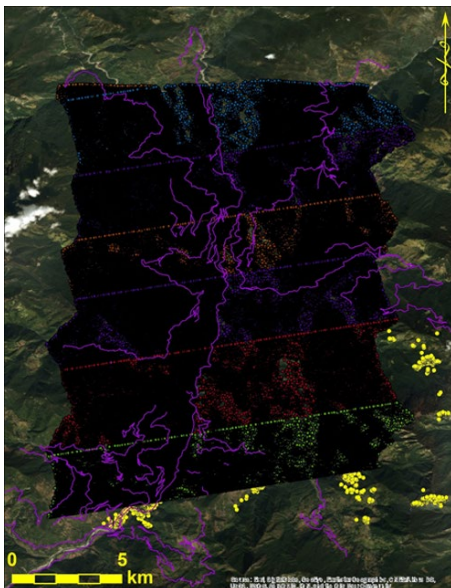


*Figure 6.*

*The entire set of original PS points processed for site 1 in India*

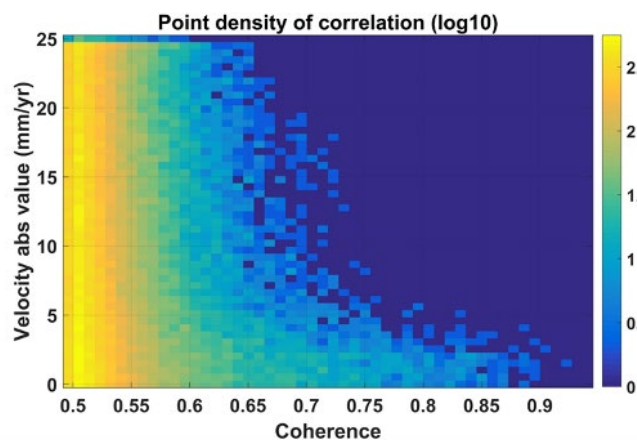


*Figure 7.*

*Two-dimensional point density map for velocity and coherence of PS points processed for site 1*

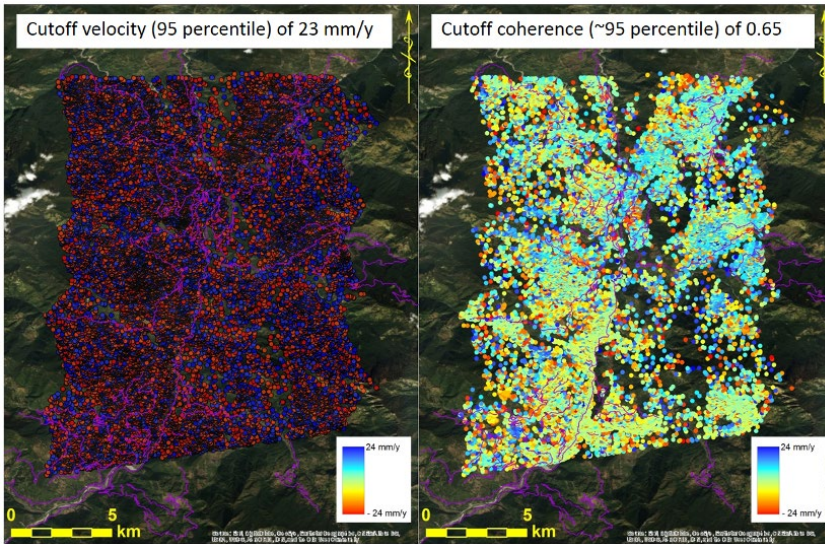


*Figure 8.* PS point subsets from the entire set of PS points processed for site 1, chosen according to two individual criteria: having velocities above the 95th percentile ( $> 23$  millimeters/year), shown in the left panel, and having a coherence also above 95th percentile ( $> 0.65$ ), shown in the right panel.

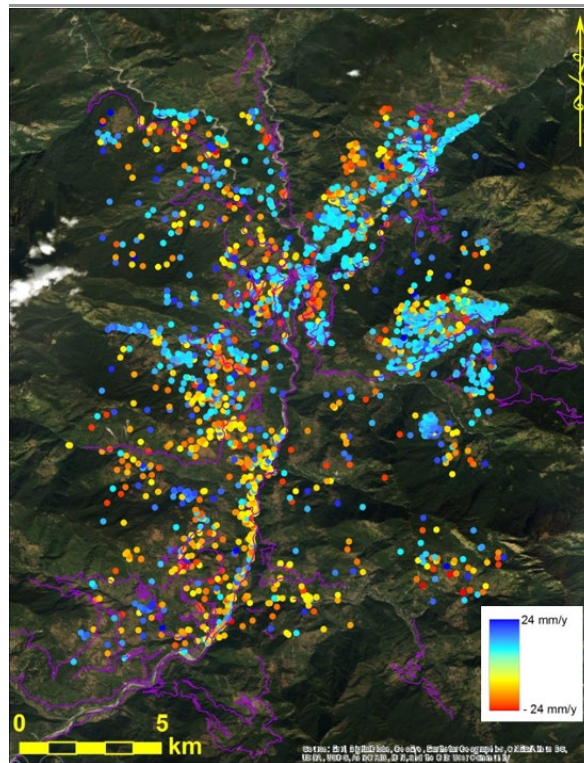


*Figure 9.* PS point subsets from the total set of PS points processed for site 1, chosen according to the same criteria as described in figure 8 but considered simultaneously: having velocities above the 95th percentile ( $> 23$  millimeters/year) and having a coherence also above the 95th percentile ( $> 0.65$ ).

Figure 8 shows the PS points selected from the total PS points set for site 1 based on two criteria: that they have velocities larger than the 95th percentile (23 millimeters/year) shown in the left panel, and that they have coherence values larger than the 95th percentile (0.65) shown in the right panel.

Choosing points based on individual criteria produces a large dataset. Instead, we decided to combine both the criteria and select those data points that fulfill both criteria simultaneously. Figure 9 shows the points that fall in that category—that is, that have a velocity ( $> 23$  millimeters/

year) and coherence ( $> 0.65$ ) that are both above the 95th percentile. The joint filtering of the PS points gives us a much more meaningful dataset that satisfies both information and quality criteria.

Once the data have been filtered, the physical meaning of the displacements and velocities must be interpreted in terms of the potential slope instability and landslide hazard. We do a first-order analysis and interpretation of the velocities by attempting to cluster them based on spatial proximity and similar velocities. The goal of clustering the

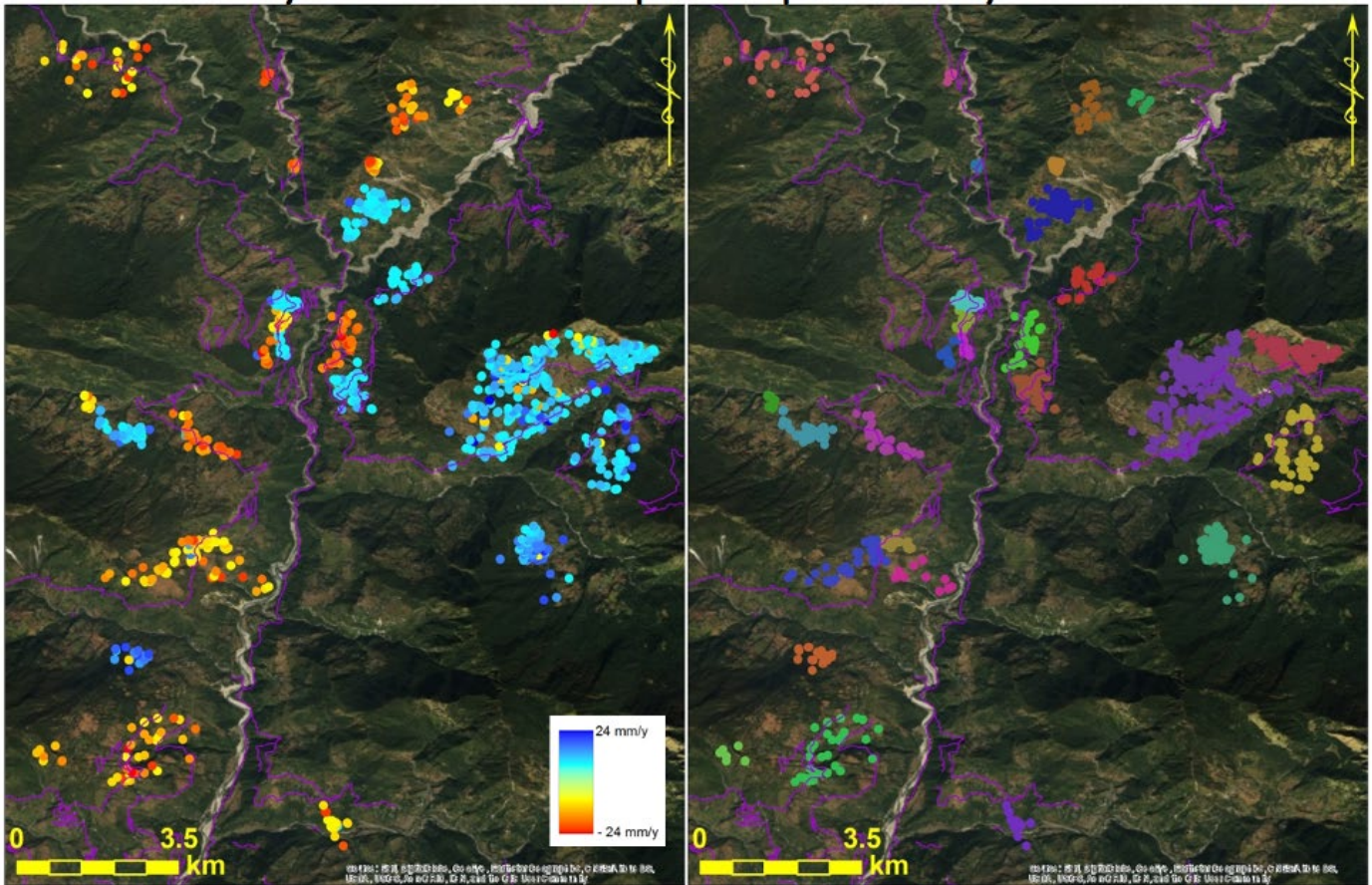


Figure 10.

Clusters of points extracted from the PS points dataset shown in figure 11. The clusters have a similar velocity (shown on the left panel), and all the points within each cluster are assigned a common identification attribute (shown on the right panel, with each color representing a cluster).

data is to identify spatial patterns in the velocity, where multiple points showing a similar velocity, which indicates a consistent slope motion. The clustering will also help to isolate individual points that behave differently from their nearby points, which could potentially reflect random or spurious displacements of the surface terrain.

Figure 10 shows the clusters obtained by this method for the same dataset shown in figure 11. Clusters show similar velocities, shown by the scale bar colors in the left panel, and are assigned a common identification attribute, shown by different colors indicating the clusters in the right panel.



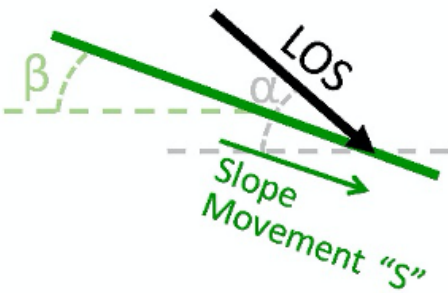
When interpreting the data, it is important to consider the meaning of the sign of the velocities and displacements. Figure 11 shows how the slope orientation and the satellite position (the look angle of the satellite) can affect the interpretation of the signs (+ve and -ve displacement). Although the absolute values of displacement and velocity are the most important pieces of information, the polarity (sign) also conveys information about slope orientation and movement direction.

Figure 11.

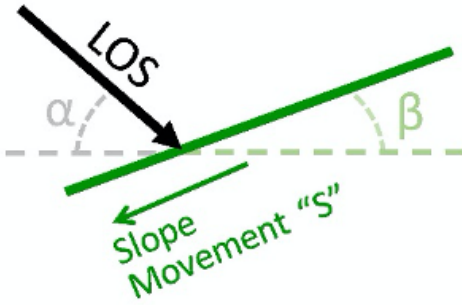
Diagram illustrating the polarity (sign) of the displacement and velocity vectors in relation to the slope orientation and the satellite viewing angle. It is also important to remember that the displacement and velocity values are only the vector component in the line of sight of the satellite.

Line of sight (LOS) inclination ( $\alpha$ ) and slope inclination ( $\beta$ ) for East and West facing slopes, for  $\alpha > \beta$ .

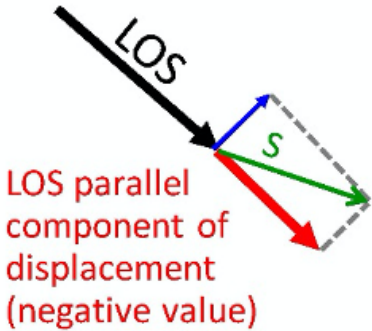
**A** East facing slope



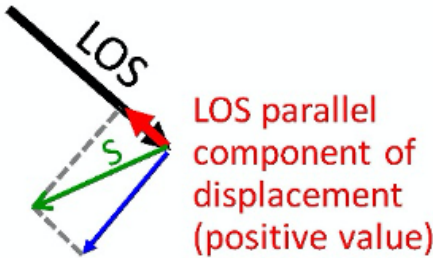
**B** West facing slope



**C** East facing slope



**D** West facing slope



# SLOPE INCLINATION IS ONE OF THE MAIN VARIABLES GOVERNING SLOPE STABILITY AND LANDSLIDING

## 4.3 HAZARD SCORING

Once the PS points have been chosen as representative of larger slope displacement potentially associated with slope instabilities and landslide hazard, we need to prioritize which areas pose the highest relative hazard to further extend the analysis to exposure (as a proxy of vulnerability) and risk. To determine these priorities, we consider the slope displacement velocity as a critical indicator of potential instability. Because of a lot of other variables also play a role in determining such a stability state (e.g., slope inclination, material strength, loads, water pore pressure, etc.), it is advisable to attempt to incorporate those that are relevant. In most scenarios, data are not available for most of these variables; the exception is terrain slope, which can easily be derived from DEMs that are available globally.

Slope inclination is one of the main variables governing slope stability and land sliding and, because of this, is used as an independent context variable to aid in ranking the hazard level for each cluster. In particular, we chose a hazard ranking method that relies on weights selected from the average velocity and slope values measured from each point cluster. Because the ranking is relative, we chose the cutoff values between weighing categories also based on percentiles. Table 1 shows an example of the criteria used for site 1.

But the relative weights of the different criteria also need to be considered, and table 2 shows the weights chosen for the clusters at site 1. In this weighting scheme, the velocity is twice as important as the slope (twice the weight), but users can choose different weights according to the site conditions. The velocity score was calculated as the velocity weight from table 1 multiplied by the relative hazard weight from table 2. The slope score was calculated similarly, as the slope weight from table 1 multiplied by the relative hazard weight from table 2. The hazard score for each cluster was then calculated as the sum of the velocity and slope scores. This is shown in equations (1) through (3).

**TABLE 1.**  
**HAZARD WEIGHTING CRITERIA USED FOR CLUSTERS IN SITE 1**

Weight	Percentile	Velocity (mm/yr)	Slope (°)
1	< 50th	23.4	11.6
2	Between 50th and 90th	23.4 to 30.0	11.6 to 18.3
3	> 90th	30.0	18.3

**TABLE 2.**  
**RELATIVE WEIGHTS OF THE DIFFERENT CRITERIA USED FOR SCORING HAZARDS**

Weight	Criteria
2	Velocity
1	Slope

### EQUATIONS 1-3

- 1. *velocity score* = velocity weight × relative hazard weight**
- 2. *slope score* = slope weight × relative hazard weight**
- 3. *hazard score* = velocity score + slope score**

## 4.4 EXPOSURE SCORING

Although *risk* properly defined would consider human vulnerability to be a critical variable, the data necessary to estimate such vulnerability are usually challenging to collect, and for this project were not available. Instead, we used physical exposure through the location as the first-order proxy for vulnerability. Locations of houses/buildings and roads near each cluster were identified visually on satellite images. Exposure of the population via the relative location of buildings and houses and the exposure of transportation infrastructure via the relative location of roads is the basis for such exposure rankings. Table 3 shows the exposure weights for different location relationships between the cluster points and houses/buildings and roads.

**TABLE 3.**  
**EXPOSURE WEIGHTING**  
**CRITERIA USED FOR**  
**CLUSTERS IN SITE 1**

Weight	Criterion
0	No houses/buildings or road downslope or upslope
1	Point cluster downslope from houses/buildings or road
2	Point cluster upslope from houses/buildings or road
3	Point cluster on houses/buildings or road

**TABLE 4.**  
**RELATIVE WEIGHTS OF THE**  
**DIFFERENT CRITERIA USED**  
**FOR SCORING EXPOSURE**

Weight	Criteria
2	Houses/buildings
1	Roads

As with hazards, the relative weights of the different exposure criteria also need to be defined, as shown in table 4. Houses and buildings have been given twice as much weight because of their importance as places where the human population is often gathered, in comparison with roads. The houses/buildings score was calculated as the houses/building weight from table 3 multiplied by the relative exposure weight from table 4. The road score was calculated similarly, as the weight of the road from table 3 multiplied by the relative exposure weight from table 4. The exposure score for each cluster was then calculated as the sum of the velocity and slope scores. This is shown in equations (4) through (6).

### EQUATIONS 4-6

**4. houses/buildings score =**  
*houses/buildings weight × relative exposure weight*

**5. roads score =**  
*roads weight × relative exposure weight*

**6. exposure score =**  
*houses/buildings score + roads score*

## 4.5 RISK PRIORITY RANKINGS

By combining the hazard and exposure ranking, a total risk ranking score was obtained. This score was calculated as the product of the hazard and exposure scores. After that, the values of all the risk scores were sorted in descending order, and a priority level was assigned to each one based on its position in the sorted table. This is shown in equations (7) and (8).

### EQUATIONS 7-8

**7. risk score =**  
*hazard score exposure score*

**8. risk priority ranking =**  
*sort from larger to smaller (risk ranking score)*

## DETAILED ANALYSIS OF KEY LANDSLIDE LOCATIONS

05

Within each study area, we looked at specific landslides that occurred during or after the time period covered by the remote sensing data that were used for the project (i.e., synthetic aperture radar, or SAR, images and high- and intermediate-resolution visible images). For such landslides, we tried to identify and measure any precursory deformation as a hindsight analysis of whether this monitoring technique could have been used at the time to forecast the potential occurrence of those landslides. The success of this approach will depend on what data are available for different periods of time and whether they coincide with particular landslides in the study areas.

### 5.1 RESULTS FOR SITE 2: ROAD NEAR REOTALA, BHUTAN

The analysis of site 2 considers four elements: persistent scatterer interferometry (PSI) processing; the results of an analysis of persistent scatterer (PS) points; the site's hazard, exposure, and risk rankings; and, finally, an evaluation of the relationship of these PS points with possible landslide areas. We present the analysis of site 2 first because it is for this site that we provide a detailed description of the relationship between the PS points and possible landslides.

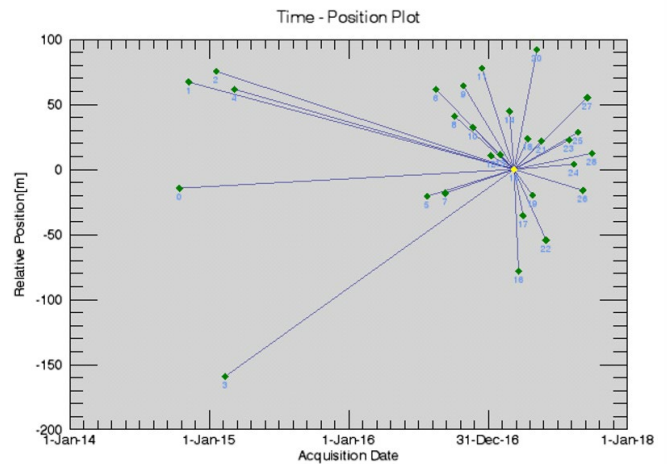


Figure 12:

Time-position plot of all 29 Sentinel-1 images used for PSI processing. This plot shows the temporal extent of radar images (acquisition date, x-axis) and relative position (y-axis) of the Sentinel-1 satellite along its orbit track in space while acquiring these images.

## 5.1.1 PSI PROCESSING

Twenty-nine Sentinel-1 images (figure 12) were first imported into ENVI SARscape (required for PSI processing). These reformatted Sentinel-1 images span 21,987 files in 60 folders and require 572 gigabytes of storage space. Since the computing time and power required to process full-sized Sentinel-1 images would require a supercomputer, these images were cut down to a smaller study area.

NASA's Shuttle Radar Topography Mission (SRTM) 30-meter digital elevation model (30-m DEM) (version 4) was downloaded over the full Sentinel-1 image areal extent and used for all Bhutan PSI processing (figure 13).

PSI processing was conducted for site 2, the road near Reotala, Bhutan, over the spatial area shown in figure 14: a polygon with an approximate area of 1,404 square kilometers. The largest city in the processing area is Trongsa

(population of 19,960);<sup>1</sup> other smaller towns and villages include Kungarapten, Changra, Lamti, and Zhemgang.

PSI processing involves a connection graph, interferometric process, inversion, and geocoding. The processing is computationally intense and can take significant time, and it is a function of the available computing capabilities. The processing time required for each step can be defined as the amount of time elapsed between the first and last files generated for that step. The processing of site 2, the road near Reotala, Bhutan, took 26 days, 20 hours, and 12 minutes and generated 486.77 gigabytes of data. Results from this PSI processing were used as the basis for all further PSI analyses for this site.

.....  
<sup>1</sup> This Trongsa, Bhutan, population estimate is based on the 2017 total population of Bhutan as reported by the National Statistics Bureau, <http://www.nsb.gov.bt/publication/publications.php?id=2>.

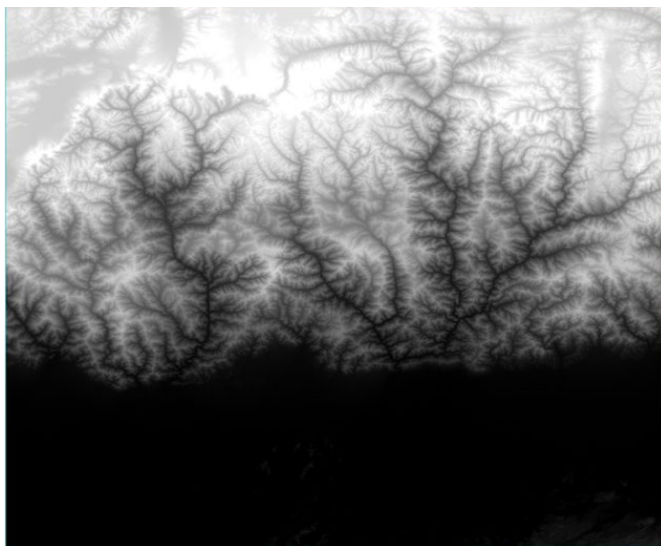


Figure 13:  
Shuttle Radar Topography Mission (SRTM) 30-meter digital elevation model DEM used for Bhutan PSI processing



Figure 14:  
Geocoded radar amplitude image covering study area with 1,404 km<sup>2</sup> spatial extent. The black outline shows the full extent of the image.

## 5.1.2 PS POINTS: FILTERING, CLUSTERING, AND DISPLACEMENT TIME SERIES

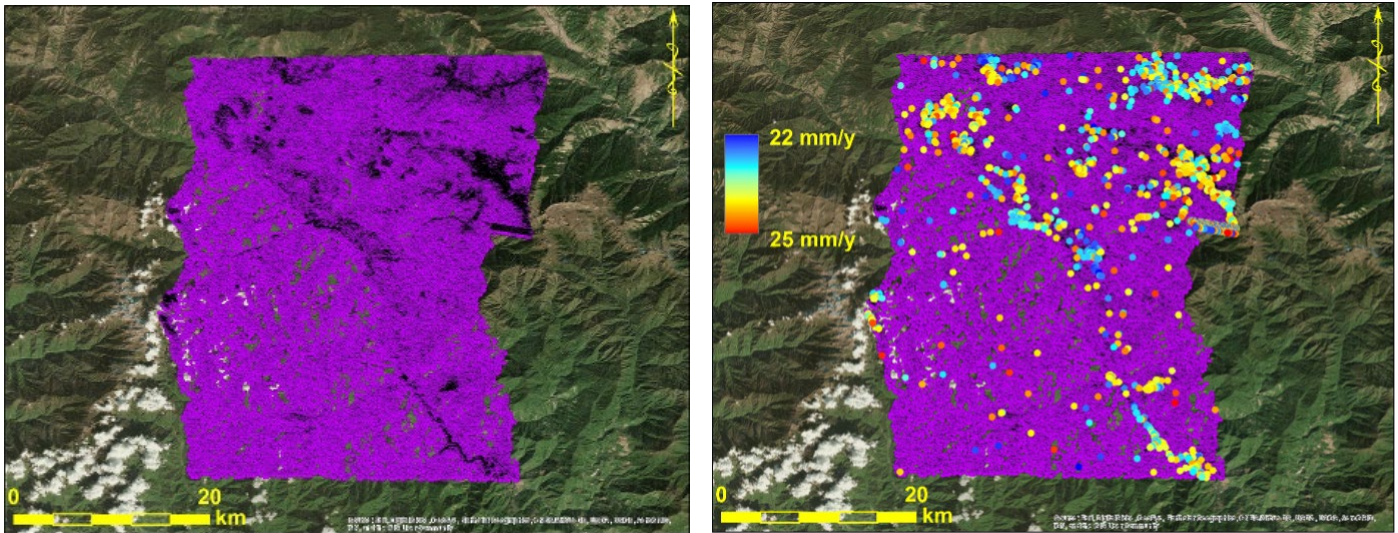


Figure 15.

The total set of PS points obtained from the InSAR processing (left) and a subset of PS points obtained from the 95th percentile criteria for velocity and coherence, shown with colors corresponding to their velocities (right)

Figure 15 shows the full PS points dataset (left panel) and the points extracted by the velocity and coherence filtering procedure (right panel). The clustering of the filtered PS points produced 45 different clusters, which are shown in figure 16. The clusters are spatially concentrated in specific locations of the study area.

The majority of the displacement time series show a linear trend without significant higher-order contributions, as shown in figures 17 through 19. The lack of accelerating trends is good news from the hazard perspective—but at the same time, the persistent displacement at a roughly constant velocity for some of the clusters should be a reason to keep monitoring those areas. The linear displacement trends also show some variability in some cases, in which a few points seem to be moving at a different speed (e.g., faster, or slower than the rest of locations). This could be caused by distinct areas that are moving somewhat independently from the rest of the slope.

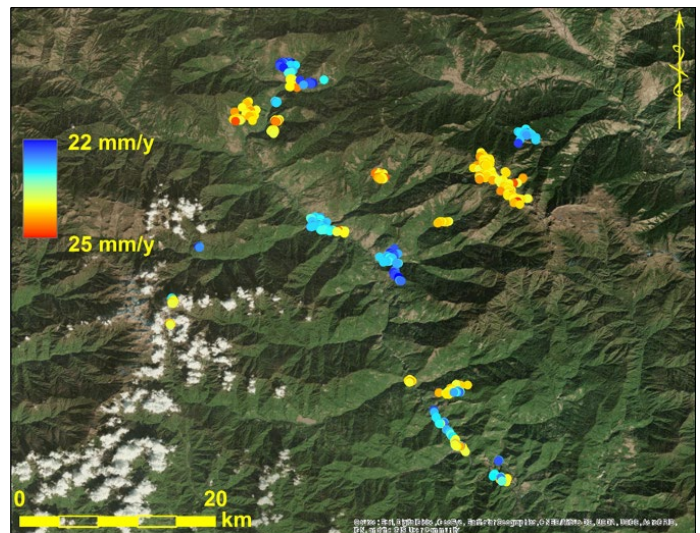


Figure 16.

PS points clusters for site 2

Figure 17.

PS displacement time series and linear regression for site 2, cluster 44

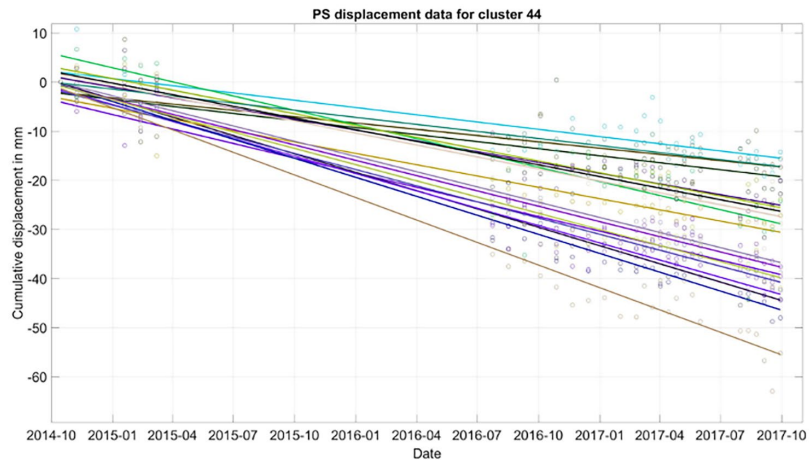


Figure 18.

PS displacement time series and linear regression for site 2, cluster 45

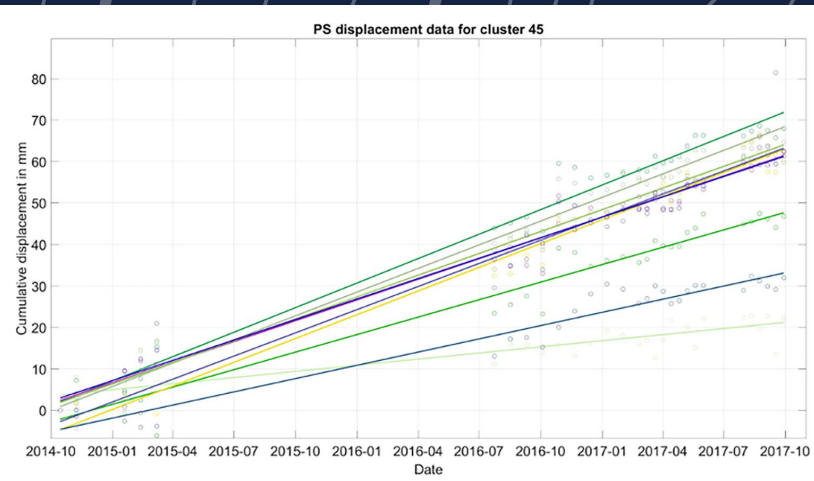
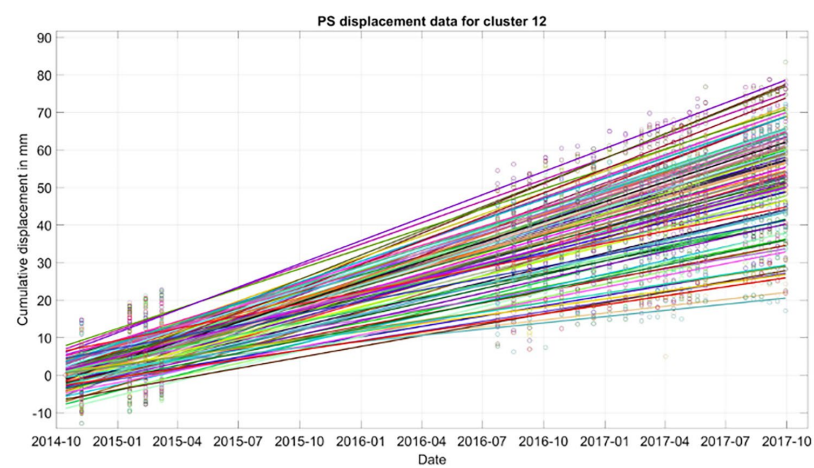


Figure 19.

PS displacement time series and linear regression for site 2, cluster 12



**SIGNIFICANT PORTIONS OF THE POPULATION AND ROAD INFRASTRUCTURE MAY BE EXPOSED TO THE HAZARDS.**

### **5.1.3 HAZARD, EXPOSURE, AND RISK RANKINGS**

In this section, we examine and discuss the hazard, exposure, and risk rankings in graphical format. The full hazard, exposure, and risk ranking values are given in the corresponding electronic appendix at the end of the report. Figure 20 shows the unweighted hazard scores for the 45 PS point clusters. Only a few have a high hazard score (score = 3) in the velocity or slope fields, and only one has a high score in both (cluster 23). The weighting of the velocity and slope hazard components has a strong effect on a few clusters in the case of the velocity score, as seen in figure 20. The total combined hazard score, which is the sum of the weighted velocity and slope scores can also be seen graphically in figure 20. Not surprisingly, cluster 23 has the highest hazard score, although the highest hazard score may not imply the highest risk.

Exposure scores are shown graphically in figure 21. Individual (unweighted) and weighted scores for houses/buildings and roads are plotted against the cluster number, indicating that the proportion of areas with high exposure to the hazard for both houses/buildings and roads (score = 3) is less, reflecting perhaps lower population densities. However, from a total of 45 clusters, 10 share the highest exposure score, which shows that significant portions of the population and road infrastructure may be exposed to the hazards.



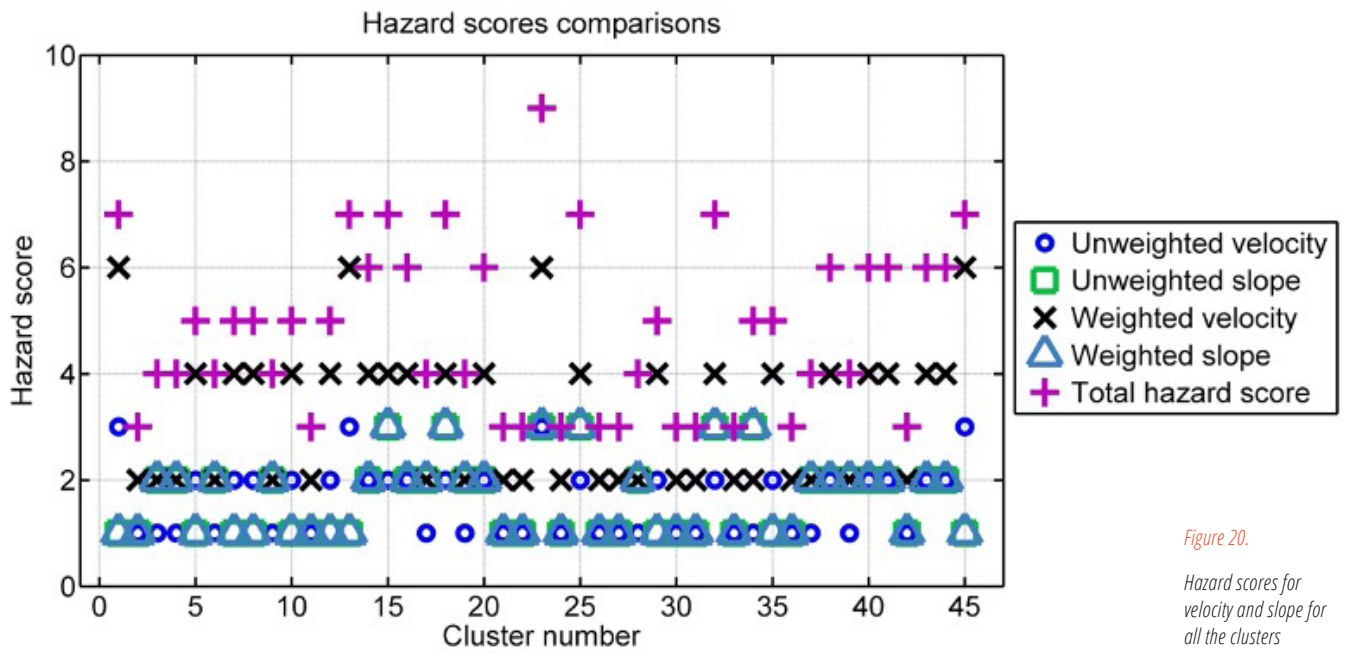


Figure 20.

Hazard scores for velocity and slope for all the clusters

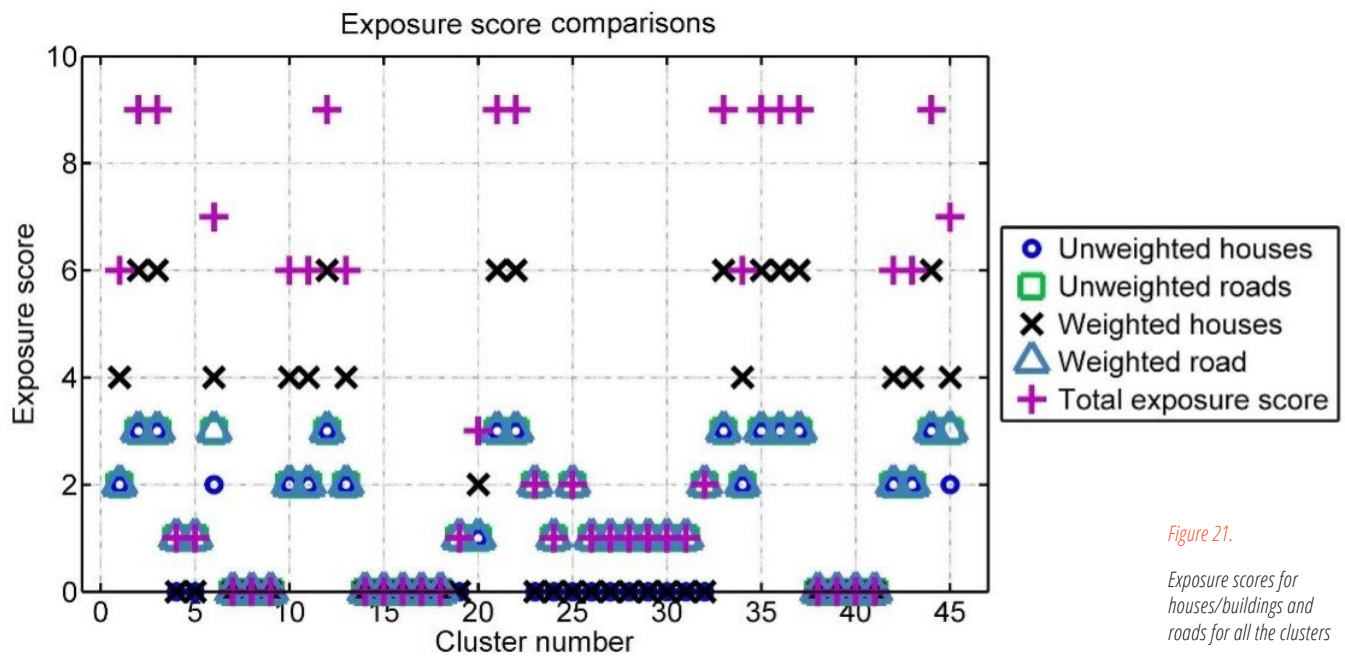


Figure 21.

Exposure scores for houses/buildings and roads for all the clusters

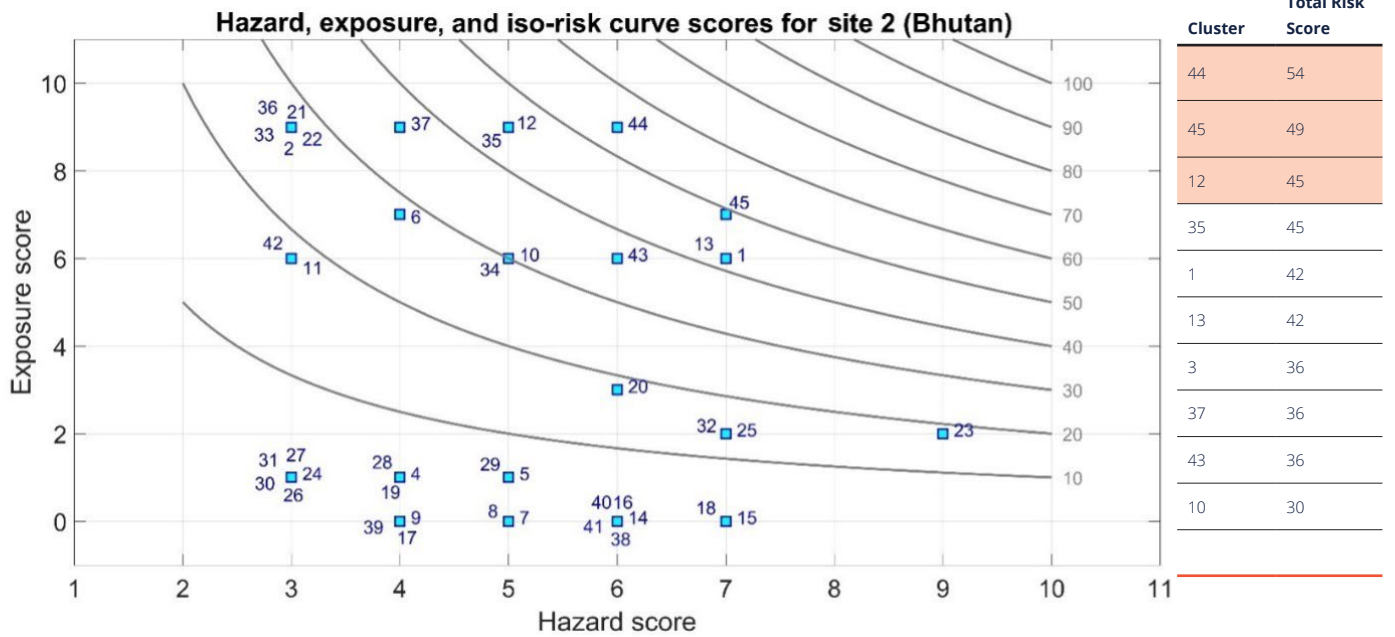


Figure 22.

Total risk scores for all the clusters. The numbers correspond to the cluster number and the squares represent their hazard and exposure scores. The darker gray line represents the iso-risk curve and shows the relative position of each cluster to the iso-risk curve.

**TABLE 5.**  
**RISK SCORES FOR THE 10 HIGHEST SCORED CLUSTERS**

The combined risk score obtained from the multiplying the hazard and exposure scores is shown in figure 22. The cluster numbers are given next to the square symbols and the gray lines represent curves with the same risk score value.

The numerical results for the 10 highest risk scores are shown in table 5.

The three highest risk ranking clusters are shown in figures 23 through 25 overlaid on high-resolution satellite images.

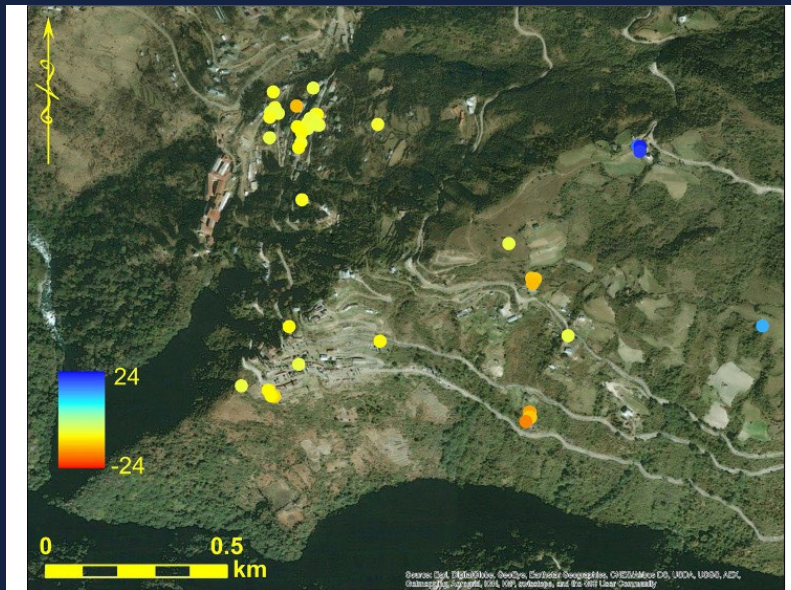


Figure 23.  
Cluster 44, which has the highest risk rank

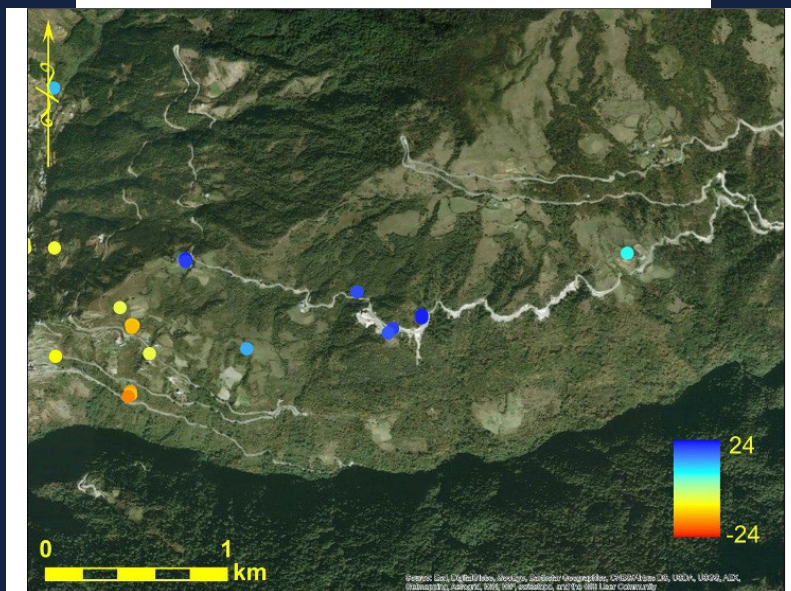


Figure 24.  
Cluster 45, which has the second highest risk rank

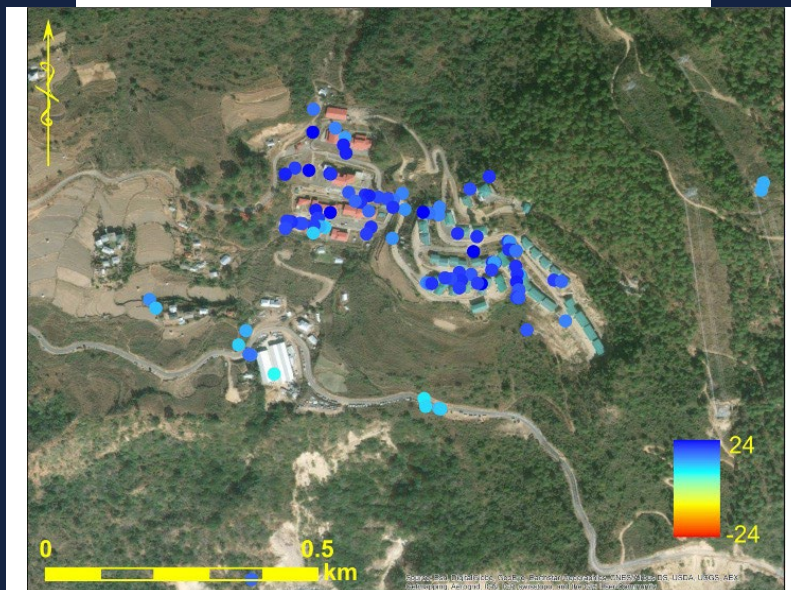


Figure 25.  
Cluster 12, which has the third highest risk rank

### 5.1.4 RELATIONSHIP WITH POSSIBLE LANDSLIDE AREAS

This section evaluates the relationship between the PS point clusters and landslides that occurred in the area during the period of monitoring. Although there seem to have been landslides in the area, most of the ones recognized in high-resolution satellite images seem to be associated with roads or road construction. The observed mass wasting processes may also be just the dumping of cut or fill material from the road construction process, or erosion associated with these processes. Figures 26 and 27 demonstrate that near the PS clusters, several recent landslide features are observed in November 2014 and October 2017 images from Google Earth. To detect these potential landslides along the roads, continuous monitoring using InSAR data will be required. Figure 28 compares an area close to the PS clusters for three different dates from 2006 to 2017. It is evident in the 2017 images that several landslide features have formed in this area. Some development activities in the area are also evident, including new roads and road widening. It is not clear whether these recent landslides are related to the development activity or whether they were triggered by other external triggering events.

**TO DETECT THESE POTENTIAL LANDSLIDES ALONG THE ROADS, CONTINUOUS MONITORING USING INSAR DATA WILL BE REQUIRED.**

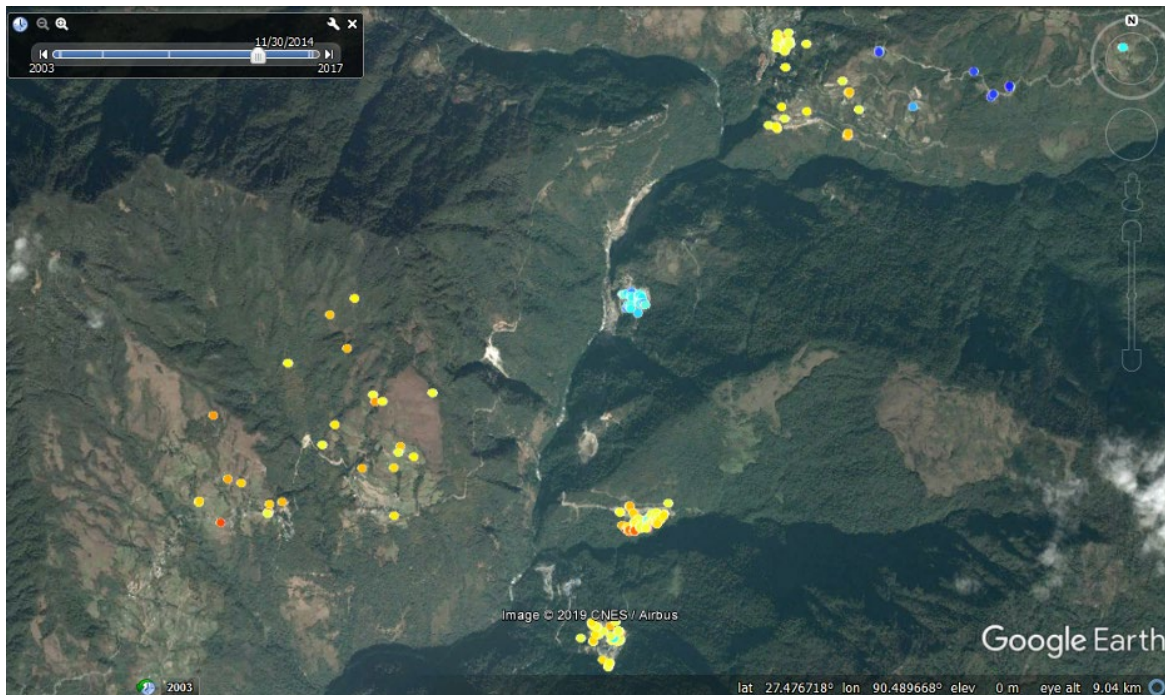


Figure 26.

Clusters near the north end of the study are shown in a satellite image  
Source: Google Earth, November 2014.

Figure 27.

Clusters near the north end of the study are shown in a high-resolution satellite image

Source: Google Earth, October 2017.

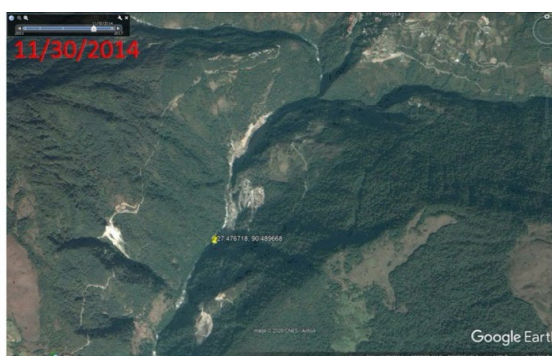
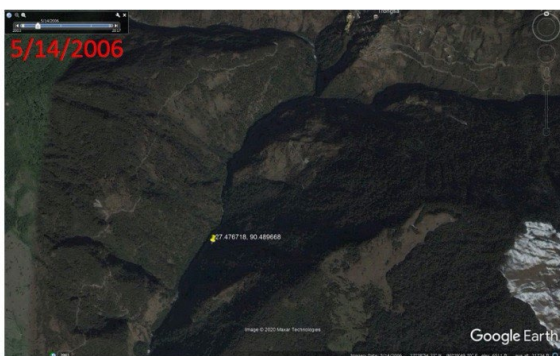
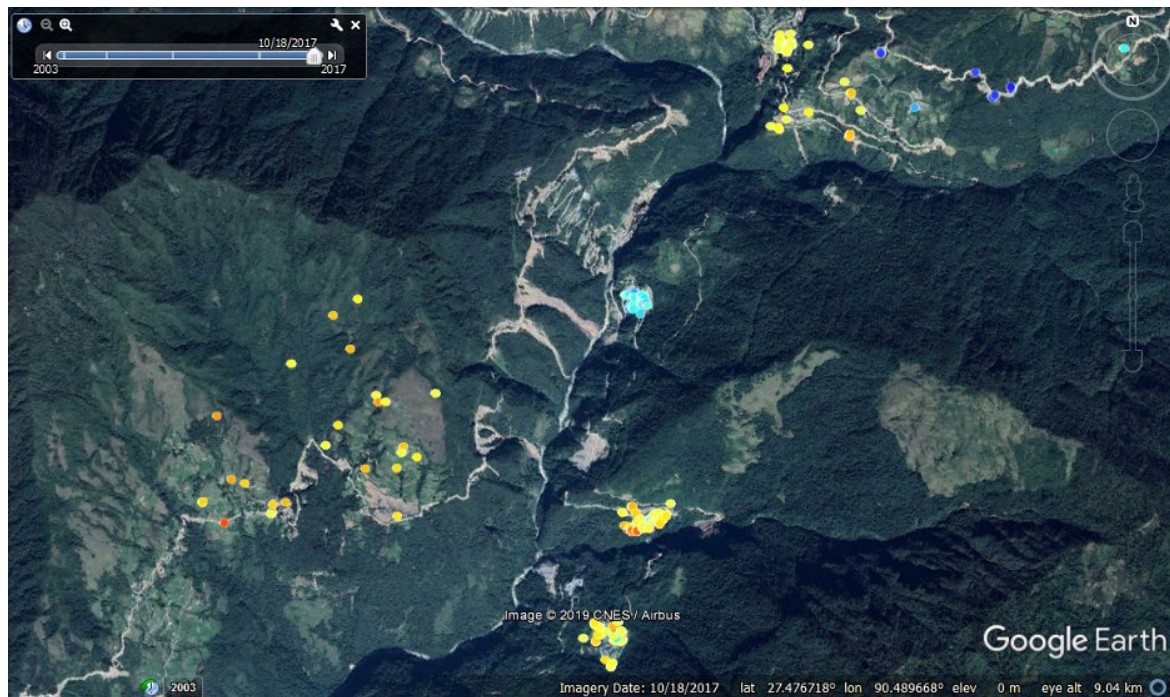


Figure 28.

A comparison of an area close to the PS cluster for three different dates from 2006 to 2017. Several landslide features are seen in the 2017 image.

Source: Google Earth, May 14, 2006; November 30, 2014; October 18, 2017.

## 5.2 RESULTS FOR SITE 1: ROAD NEAR RUDRAPRAYAG, INDIA

### 5.2.1 PSI PROCESSING

PSI processing was conducted for Site 1, the road near Rudraprayag, India. Twenty-nine Sentinel-1 images were processed from India. NASA's SRTM 30-m DEM (version 4) was downloaded over the full Sentinel-1 image areal extent and used for the PSI processing of India data over a polygon with an approximate area of 268 square kilometers (figure 29). Villages in the processing area include Jola (population 2,503); Temriya (population 2,772); Chandrapuri (population 201); Agastmuni or Rudraprayag (population 242,285), and almost as far north as Tarsali (population 26,709).<sup>2</sup>

### 5.2.2 PS POINTS: FILTERING, CLUSTERING, AND DISPLACEMENT TIME SERIES

Figure 30 shows the full PS points dataset (left panel) and the points extracted by the velocity and coherence filtering procedure (right panel). From an initial 606,075 PS points, only 2,765 were selected after velocity and coherence filtering. Those points were subjected to the cluster analysis procedure, which produced 28-point clusters (see figure 31) with relatively high velocities and compact grouping, representing a final total number of 1,831 points in those clusters. The majority of the displacement time series show a predominantly linear trend, as can be seen in the example shown in figure 32.

<sup>2</sup> India population figures are based on the country's 2011 census, <https://censusindia.gov.in/>

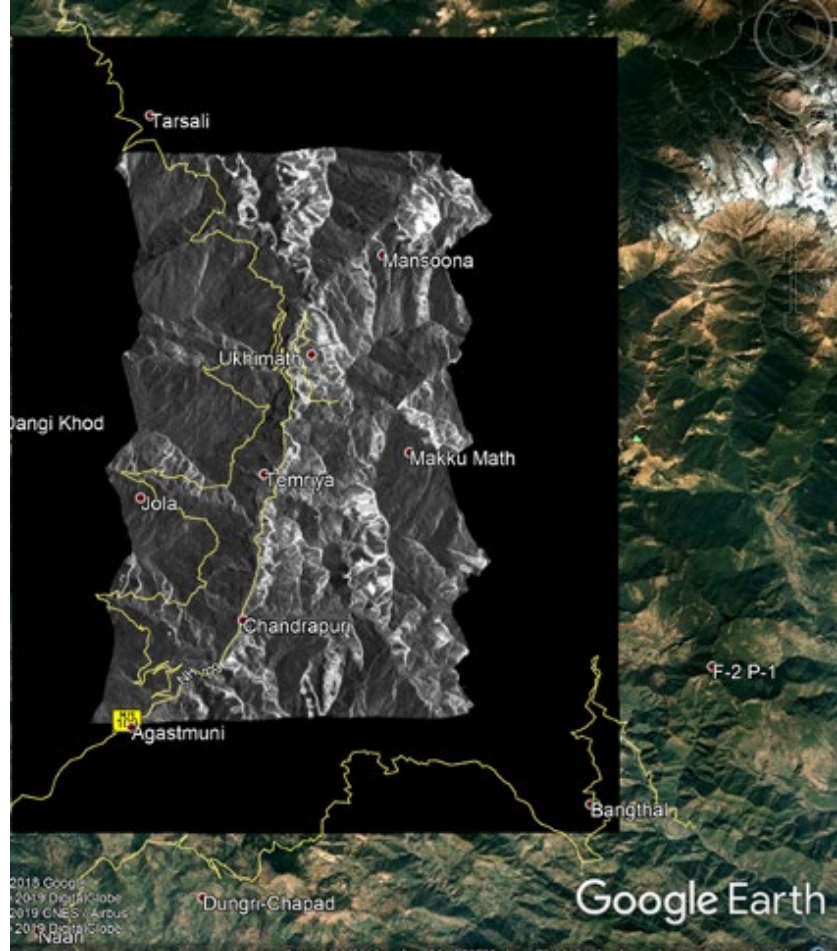


Figure 29. Geocoded radar amplitude image. PSI processing spatial extent, approximately 268 km<sup>2</sup>. The black outline shows the full extent of the image. Source: Google Earth.

THE MAJORITY OF  
THE DISPLACEMENT  
TIME SERIES SHOW  
A PREDOMINANTLY  
LINEAR TREND

Figure 30.

Complete PS points (left panel) and extracted PS points (right panel) after velocity and coherence filtering

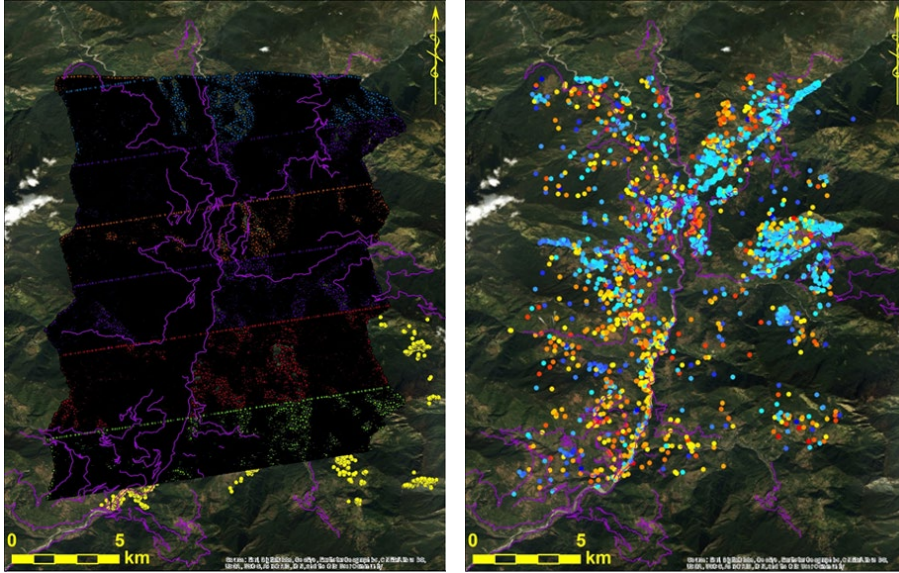


Figure 31.

PS points showing the displacement value

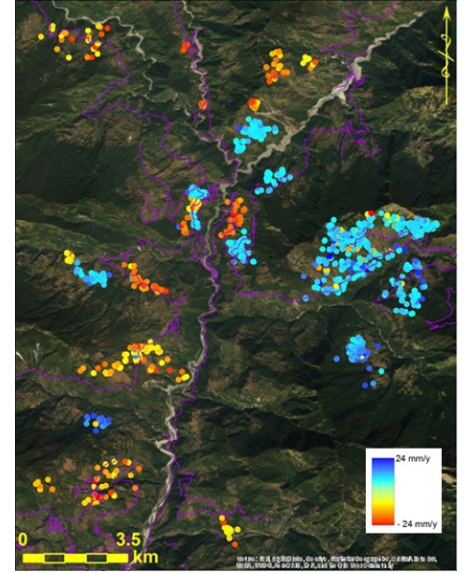
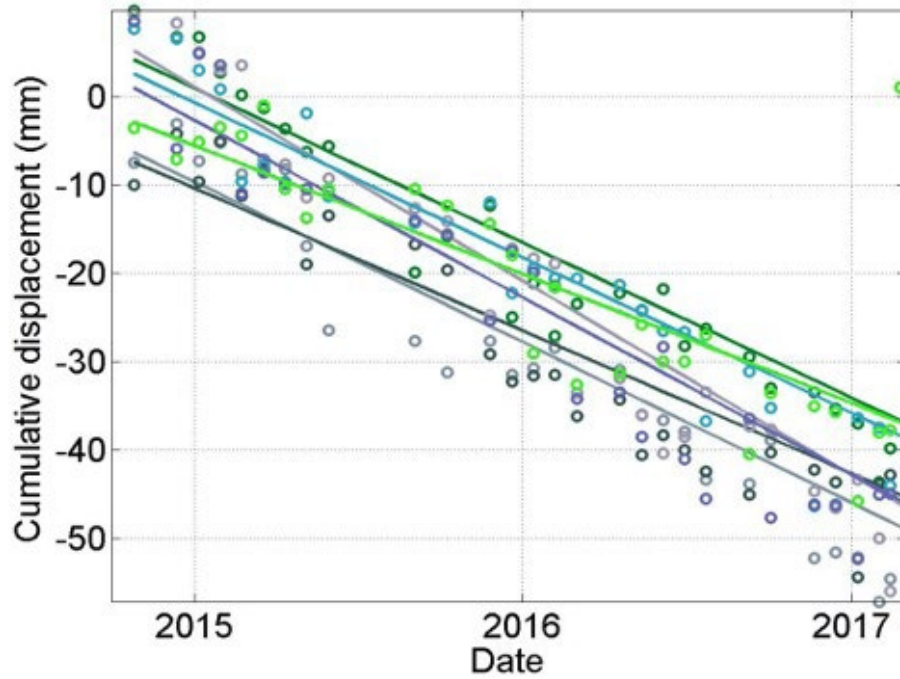


Figure 32.

PS displacement time series and linear regression for site 1

Cumulative deformation (mm) over the study period at cluster 1



### 5.2.3 HAZARD, EXPOSURE, AND RISK RANKINGS

Combining the final hazard and exposure scores gives the risk scores that are used to rank and prioritize the clusters by their risk status. Figure 33 shows the final risk scores for all clusters as a function of both the hazard and exposure scores. The cluster numbers are given next to the square symbols, and the gray lines represent curves with the same risk score value.

The numerical results of the risk scoring can be seen in table 7 for the 10 highest hazard scores. The full list of all values is given in the electronic appendix. Figure 34 shows the three highest-ranking clusters over a high-resolution satellite image from Google Earth.

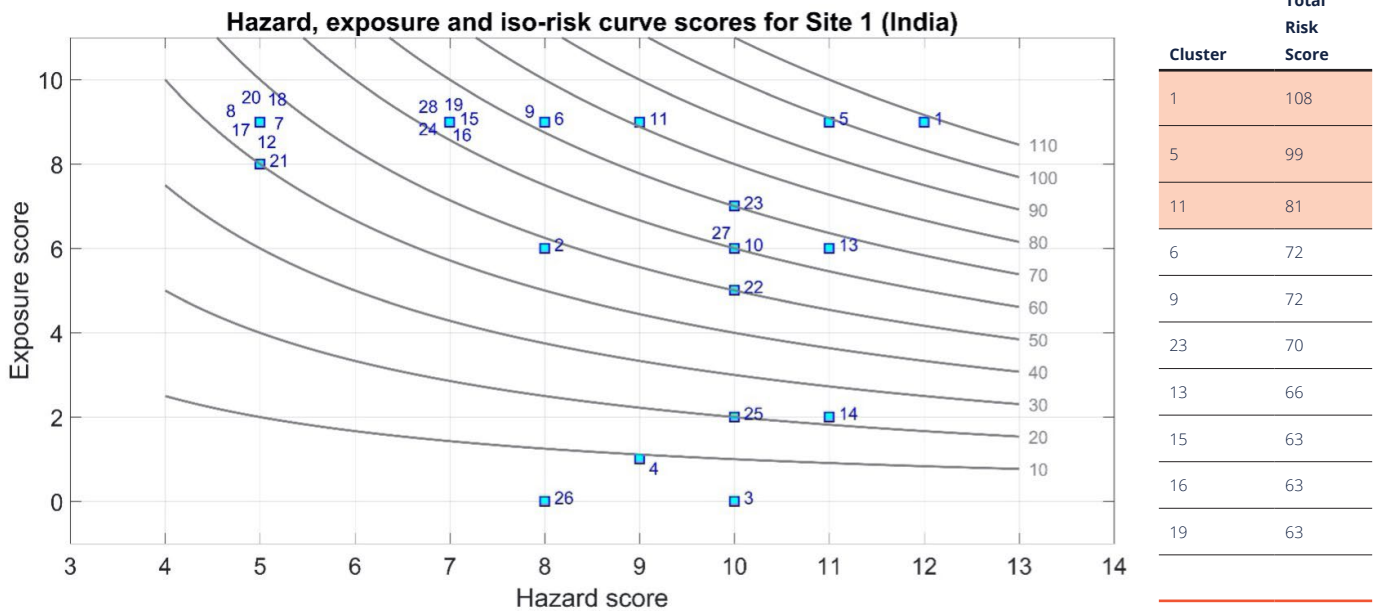


Figure 33. Individual risk scores for all the clusters

TABLE 6. RISK SCORES FOR THE 10 HIGHEST SCORED CLUSTERS



COMBINING THE FINAL HAZARD AND EXPOSURE SCORES GIVES THE RISK SCORES THAT ARE USED TO RANK AND PRIORITIZE THE CLUSTERS BY THEIR RISK STATUS.

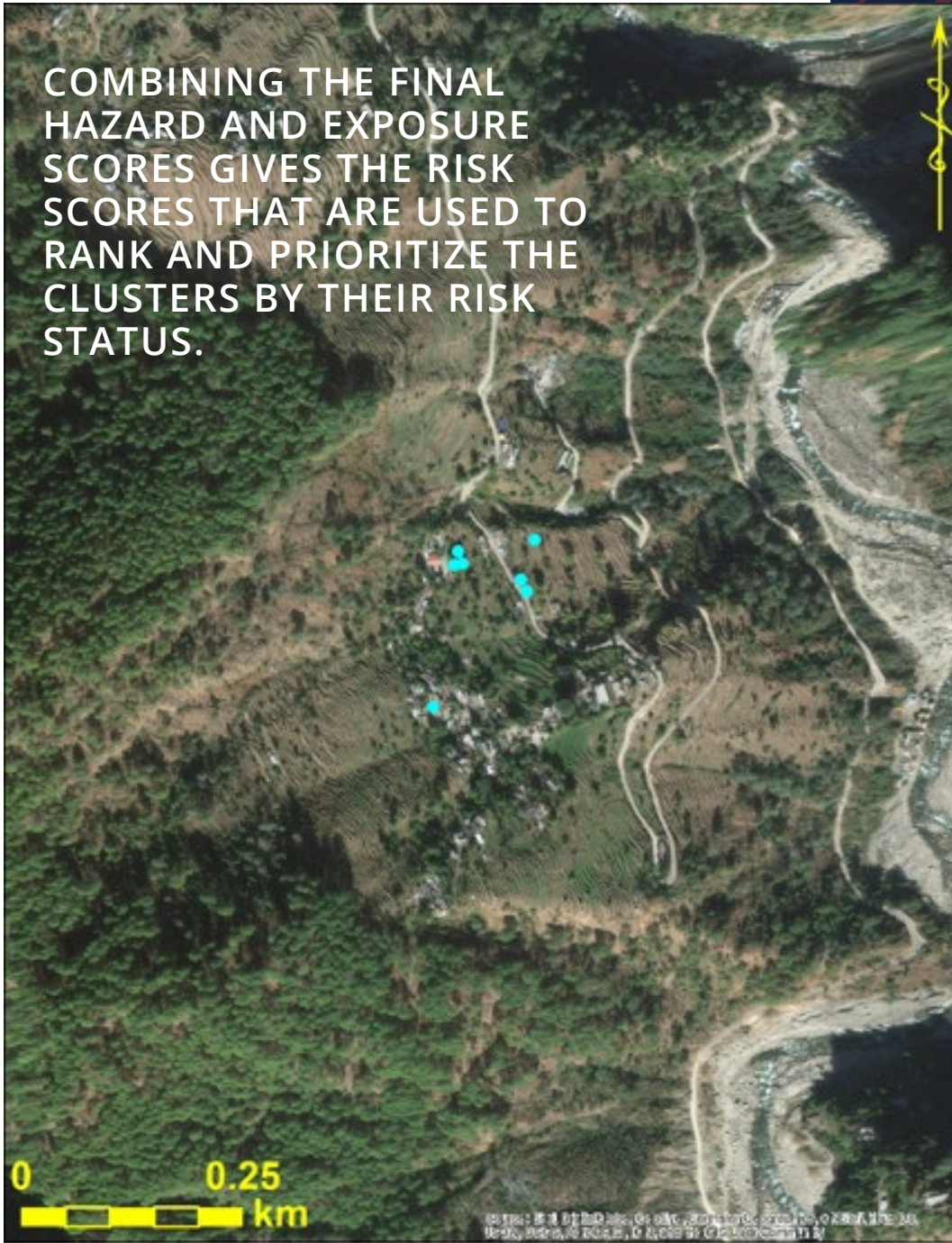


Figure 34.

Cluster 1, which also happens to be the cluster with the highest risk rank

Source: Google Earth.

## 5.3 RESULTS FOR SITE 3: ALONG THE RAPTI HIGHWAY (ROAD H11 NEAR SHARADA) NEPAL

### 5.3.1 PSI PROCESSING

Twenty-seven Sentinel-1 images were processed from Nepal. NASA's SRTM 30-m DEM (version 4) was downloaded over the full Sentinel-1 image areal extent and used for all Nepal PSI processing.

PSI processing was conducted for Site 3: Along the Rapti Highway (Road H11 near Sharada) Nepal over the spatial area shown in figure 35, a polygon with an approximate area of 370 square kilometers. Towns and villages in the processing area include Sharada (population 23,730); Saijuwal Takura (population 3,137); Kajeri (population 3,998); and Syanikhal (population 3,711).<sup>3</sup>

### 5.3.2 PS POINTS: FILTERING, CLUSTERING, AND DISPLACEMENT TIME SERIES

From a very large initial dataset, the 95th percentile velocity and coherence filtering produced a subset of points. PS points clustering further reduced the filtered PS points into a set of 70 different clusters, as shown in figure 36.

<sup>3</sup> Population numbers are taken from the Nepal Census data for the population as of 1991, <https://unstats.un.org/unsd/demographic-social/census/documents/Nepal/Nepal-Census-2011-Vol1>.

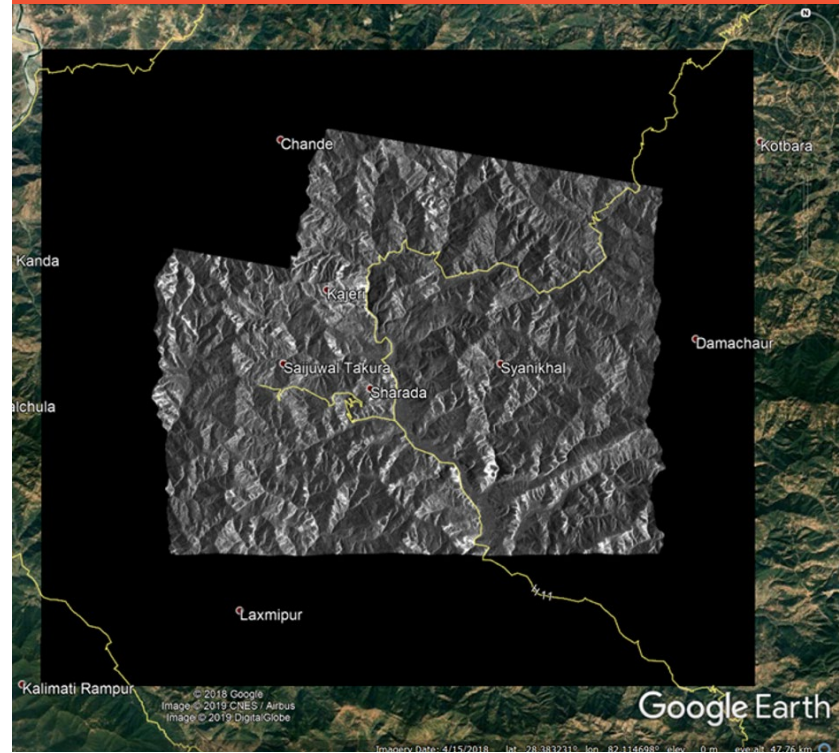


Figure 35.

Geocoded radar amplitude image covering study area with 370 km<sup>2</sup> spatial extent

Source: Google Earth, April 15, 2018

The regression of cumulative displacement with respect to time for one cluster is shown in figure 37. Linear trends dominate the cumulative displacement time series, which suggests a broadly constant velocity. The lack of accelerating trends (upward concavity) in the time series is good from the risk perspective, as an accelerating slope would be much more concerning than a slope showing constant velocity movement. For the most part, the velocities remain similar for different points within a cluster. Still, some exceptions deviating from the rest of the points in the cluster and having different regression lines (different velocities) are observed. Such points may correspond to portions of the slope moving somewhat independently from the rest of the slope.

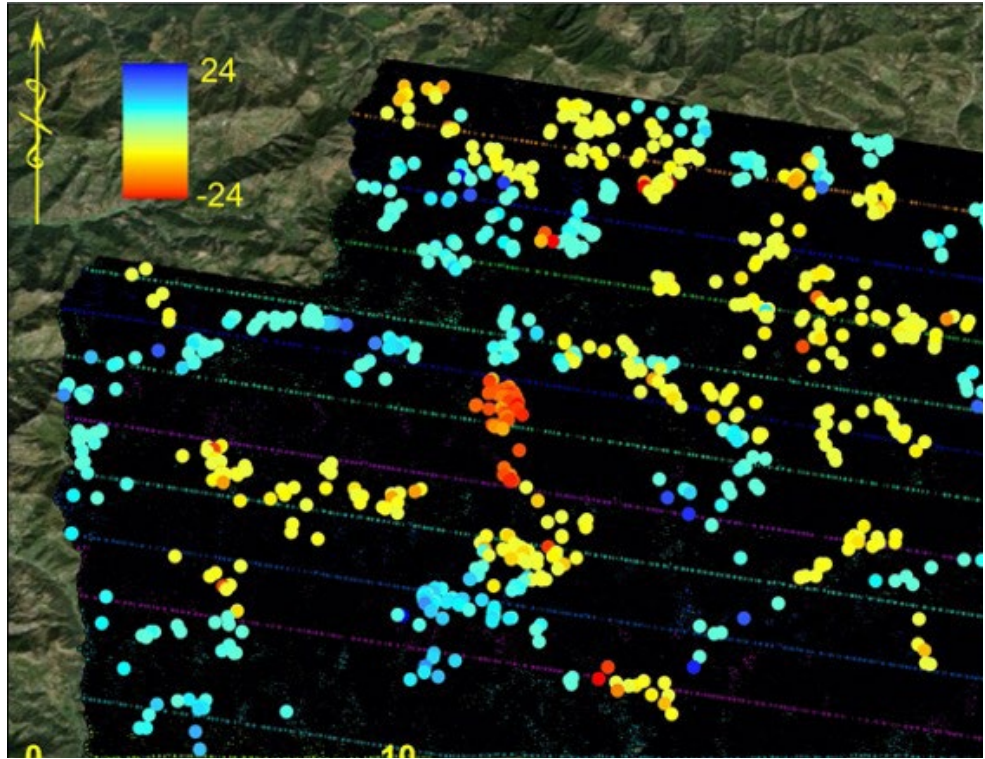


Figure 36.

PS points after cluster analysis for site 3

### Cumulative deformation (mm) over the study period at cluster 7

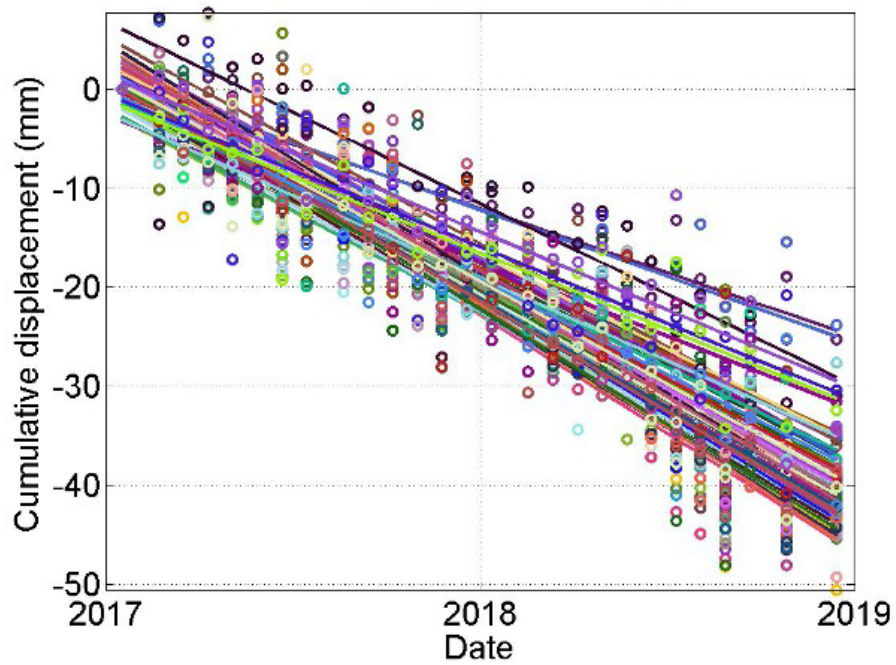


Figure 37.

PS displacement time series and linear regression for site 3, cluster 7

### 5.3.3 HAZARD, EXPOSURE, AND RISK RANKINGS

Taking the combined scores of the hazard and exposure variables, a total (combined) risk score can be assigned to each cluster, as shown graphically in figure 38. The cluster numbers are given next to the square symbols, and the gray lines represent curves with the same risk score value. The risk scoring results for the 10 highest scores can be seen in table 6. The map for the cluster with the highest risk scores are shown in figure 39.

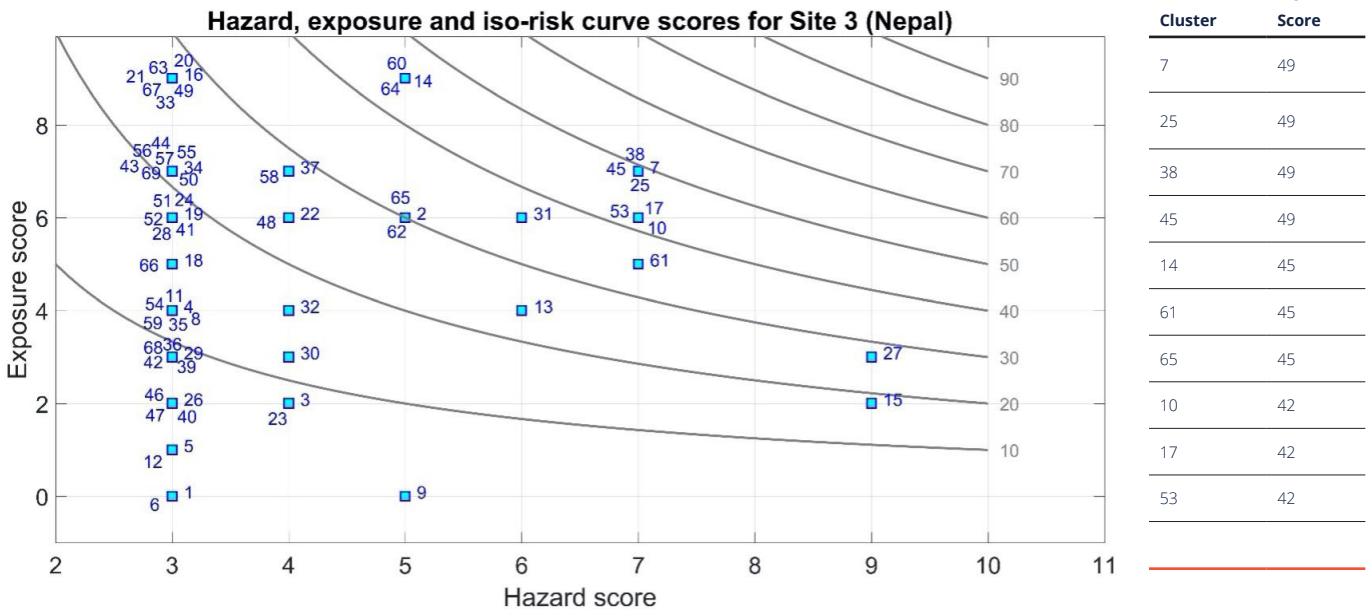


Figure 38. Exposure scores for houses/buildings and roads for all the clusters.

**TABLE 7.**  
**RISK SCORES FOR THE 10 HIGHEST SCORED CLUSTERS**

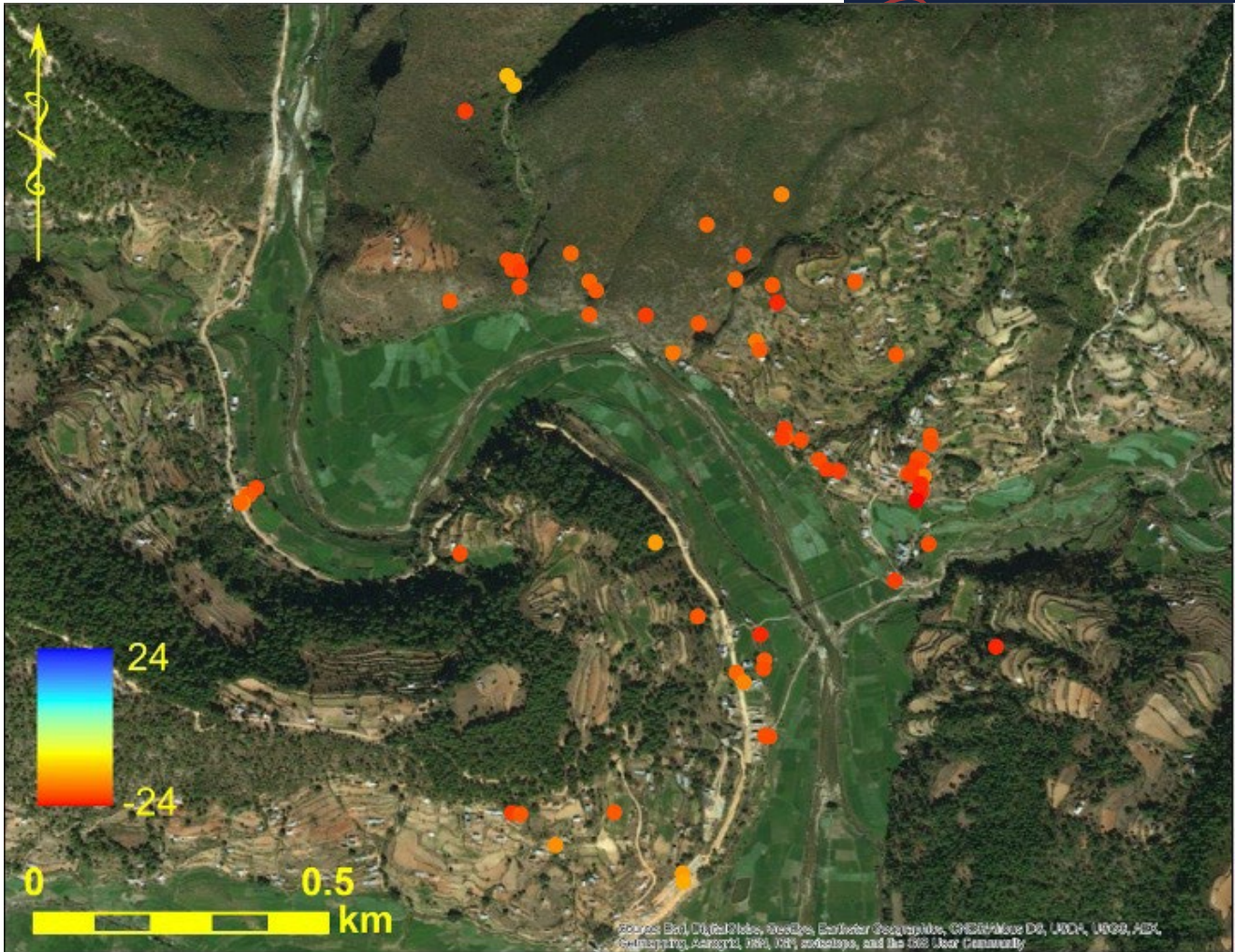


Figure 39.

Cluster 7, which has the highest risk rank site in Nepal

**TAKING THE COMBINED SCORES OF THE HAZARD AND EXPOSURE VARIABLES, A TOTAL (COMBINED) RISK SCORE CAN BE ASSIGNED TO EACH CLUSTER**

---

## IN SITU MONITORING AND VALIDATION

---

06

### 6.1 INTRODUCTION

The Project for Capacity Development on Countermeasures of Slope Disaster on Roads in Bhutan implemented by the Japan International Cooperation Agency (hereafter, the JICA Project) utilized the outcomes of the WB Project. Primarily, the JICA Project employed the critical sites identified from the WB Project's remote sensing for the pilot site selection.

The JICA Project has been ongoing since December 2018 to develop the road disaster prevention capacity of the Ministry of Works and Human Settlement, the Department of Roads (DoR), in Bhutan. In the JICA Project, Japan's technology for structural and non-structural countermeasures against slope disasters is being transferred to Bhutan. Among the non-structural countermeasures being transferred is Japan's method of ex ante traffic control based on rainfall. At present, on Japanese expressways and national roads, a rainfall threshold is established for ex ante traffic control for each set section, rainfall is monitored in real-time, and a system is established in which ex ante traffic control can be implemented immediately after the rainfall threshold is exceeded (West Nippon 2015; Ministry of Land 2020). These rainfall thresholds are determined based on past disaster history and rainfall at the time of disaster occurrence.

After establishing a rainfall threshold, critical slopes are identified, countermeasures are designed, and slope monitoring systems are established (Ministry of Land 2002).

In Bhutan, disaster history recording, and rainfall monitoring are limited. Therefore, it is important to start by boosting the capacity for such monitoring in order to set the rainfall threshold for ex ante traffic control. In order to record disasters and observe rainfall, the JICA Project has installed automated rain gauges and slope tilt sensors to detect slope failures on road slopes in Bhutan. This slope monitoring has been implemented since April 2019. This chapter introduces the methods of slope monitoring implemented in the JICA Project, the monitoring results obtained during the rainy season in 2019, and the future plan of the JICA Project.

### 6.2 METHOD OF SITE SELECTION AND SLOPE MONITORING

#### 6.2.1 SELECTION OF THE PILOT SITES

In the JICA Project, pilot sites for conducting slope monitoring were selected for Primary National Highway No. 1 (PNH 1), which is the key to east-west traffic in Bhutan, and for Primary National Highway No. 4 (PNH 4), which is one of the main roads leading to India. The selection procedure and results are detailed here.

1 In the JICA Project, a long list of potential pilot sites for slope monitoring was created with reference to high-risk priority points identified in the WB Project. In the WB Project, from 2014 to 2017, the amount of deformation of houses/buildings and the ground surface was measured by satellite monitoring using PSI (Oommen 2019) in mountainous areas, including PNH 1 and PNH 4 in Bhutan. Points with a high deformation



Figure 40:

Location map of the pilot sites. The circles on the map indicate the PS (persistent scatterer) points. The color bar at the left shows the deformation velocity of the PS points.

velocity and a relatively steep slope were selected as high-risk priority points. PSI is excellent for observing the deformation of a location such as a house/building or a bedrock, where the coherence does not decrease for a long time and reflects a stable signal. On the other hand, it is not suitable for observing points where the shape of the surface tends to change, such as trees change by season. At such points, accurate deformation may not be observed. Therefore, in the JICA Project, locations near historic landslide blocks—including the high-risk priority points identified from the WB Project—were selected under the assumption that there is a higher hazard for slope disasters in the area near the high-risk priority points. The selection was made with the results of an interpretation that used a satellite image and a topographical map created from NASA's Shuttle Radar Topography Mission (SRTM) 30-meter digital elevation model (30-m DEM) (version 4), which was used for the persistent scatterer interferometry (PSI) procedure in the WB Project. After this procedure, a site survey was conducted with the DoR staff and the JICA Project team, which resulted in selecting eight road slopes (shown in red letters in figure 40) as a long list, where slope disasters occurred recently in the landslide blocks.

2 Road slope disaster inspection (Shigeki and Toshimi 2006) was conducted for the selected slopes to evaluate the potential impact of landslide on road traffic based on the slope width, slope height, slope inclination, status of

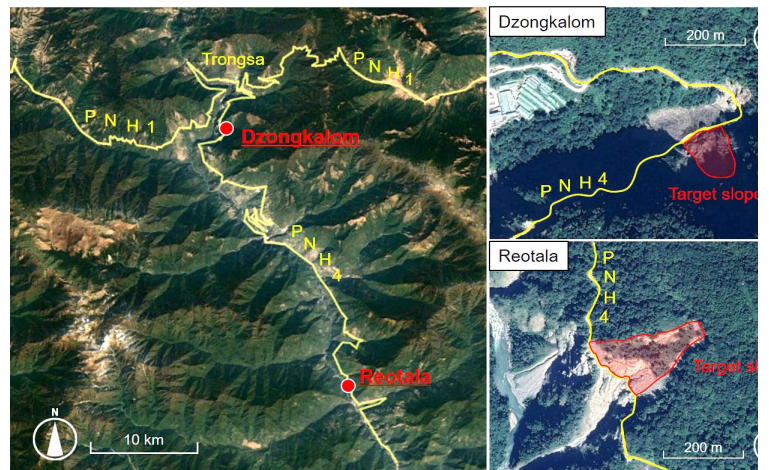


Figure 41:

Location map of the pilot study sites

the unstable soil, and status of the countermeasures of mitigation work done to stabilize the slope. Furthermore, a shortlist was created after a comprehensive evaluation, including the results of the road slope disaster inspection, and the following conditions were confirmed on each site:

- There is space on the slope to safely install the slope tilt sensor.
- There is an access route that can safely reach the installation location.
- There is space to install a rain gauge and base station.

As a result of this narrowing down process, four slopes were selected: Bumthang Highway, Dzongkalom, Dangdung, and Reotala.

3 The shortlisted sites were discussed with DoR. The discussion focused on the information on the disasters that have occurred frequently in recent years in these sites and the urgent measures that are required according to DoR. Based on the DoR information and its priorities, Dzongkalom and Reotala were selected as pilot sites for slope monitoring. The locations of the two chosen slopes, Dzongkalom and Reotala, are shown in figure 41.

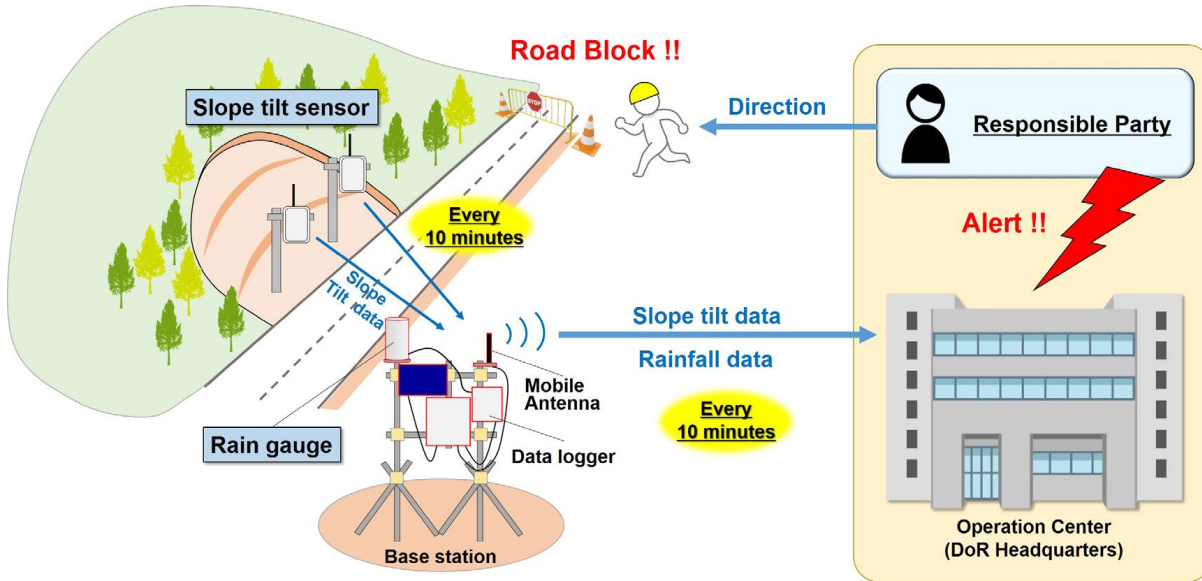


Figure 42:

Flow chart of the early warning system

## 6.2.2 BUILDING A SLOPE MONITORING SYSTEM

In the JICA Project, an early warning system has been built that—when the observed rainfall exceeds the rainfall threshold—can automatically observe rainfall, detect slope failure, collect data, and give alerts for ex ante traffic control (figure 42).

This system transmits the data acquired by the automated rain gauges and slope tilt sensors for slope failure detection to the data server installed at DoR headquarters every 10 minutes over a mobile phone connection; these data are automatically analyzed every 10 minutes. The rainfall threshold is determined based on the rainfall data and the slope tilting angle of the slope surface and is set to issue an alert 30 minutes or more before a slope failure occurs. If a slope failure is detected or the observed rainfall exceeds the rainfall threshold, a warning is issued to the responsible party at the operation center. The responsible party directs the person in charge at the site to put in place a roadblock so that the ex ante traffic control is enforced. The system can issue an alert 30 minutes or more before the expected time of the slope failure so that ex ante traffic control can be completed before the slope failure occurs.

A tipping bucket type rain gauge was used as an automated rain gauge because it has high-resolution and accurate data can be acquired with it. The measurement unit of this rain gauge is 0.5 millimeters/tipping, and its precision is within  $\pm 0.5$  millimeters when rainfall is 20 millimeters or less

and  $\pm 3$  percent when rainfall is more than 20 millimeters (figure 43).

For the mass movement observation, slope tilt sensors were used. Equipment and tools for installing slope tilt sensors are available in Bhutan, and their installation is easy because the sensors are installed on the ground's surface. In addition, since the price is relatively low, DoR can easily cope with further installations in the future. When a strain occurs on the slope, it is estimated that the angle of the slope surface will change to a considerable extent as the strain increases. If the slope change on the slope surface is the result of a mass movement, the slope tilt sensor can be used to determine the timing of the start of the mass movement and slope failure. The slope tilt sensor is installed at a depth of 50 centimeters from the surface, tied to an L-shaped angle, and fixed, in order to observe the vertical inclination. The slope tilt sensor is a 2-axis tilt sensor of X and Y, the measurement range is  $-30^\circ$  to  $+30^\circ$ , and the resolution is  $0.003^\circ$ .

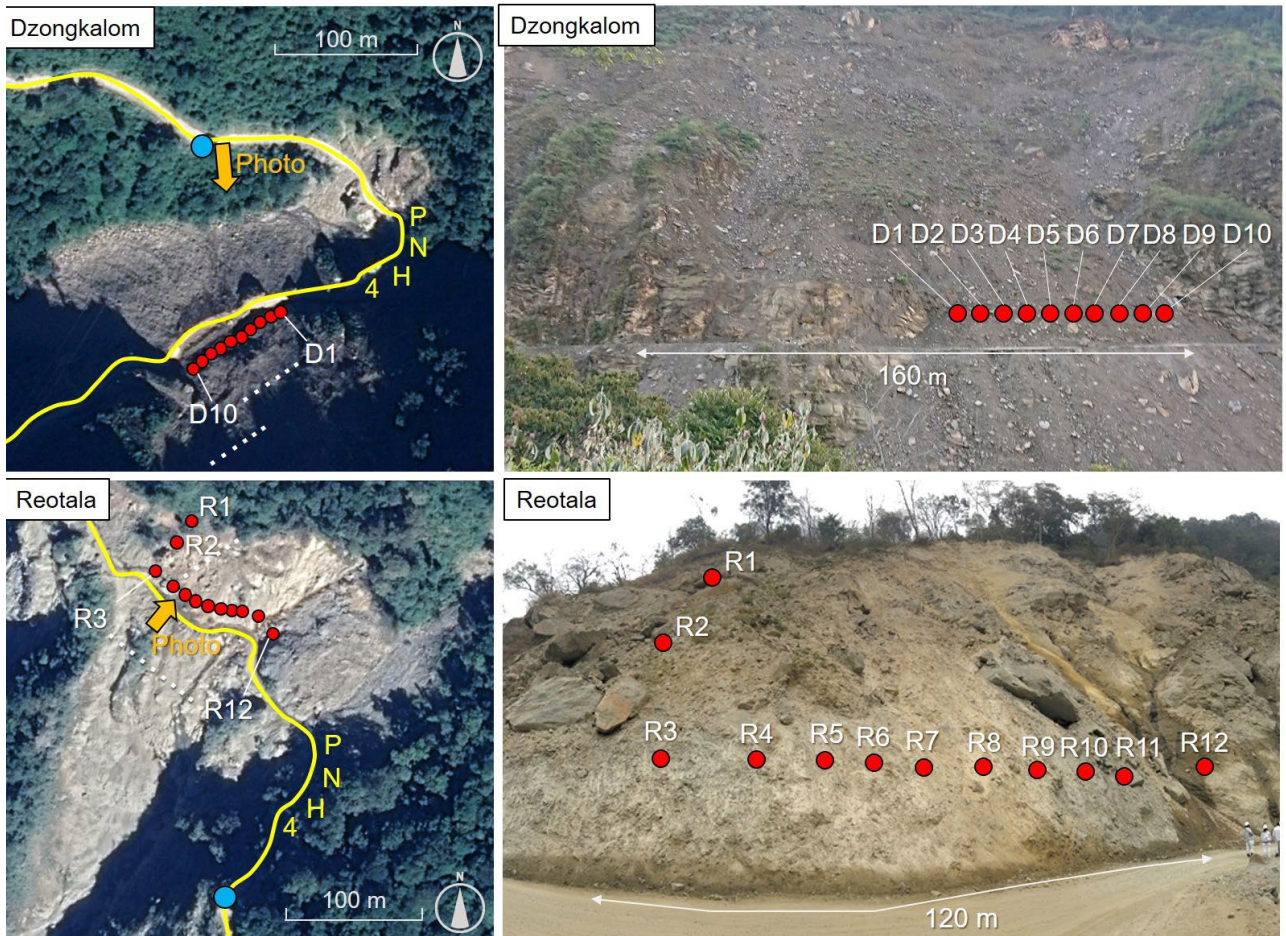
In the JICA Project slope monitoring, slope tilt sensors were installed at the angle considered to be optimal for observing the maximum tilting angle of the slope surface, which is x-axis + direction in the downward slope and - direction in the upward slope (figure 44). Moreover, the sensors were installed at the toe of the slope (besides the roads), where the slope failure would have an impact on the road.



A TIPPING BUCKET TYPE RAIN GAUGE WAS USED AS AN AUTOMATED RAIN GAUGE BECAUSE IT HAS HIGH-RESOLUTION AND ACCURATE DATA CAN BE ACQUIRED WITH IT.



Figure 43:  
Tipping bucket type rain gauge



LEGEND : ● Rain gauge ● Slope tilt sensor

Figure 44:

Arrangement of the rain gauge and slope tilt sensor  
Note: PNH 4 is Primary National Highway 4.

### 6.3 RESULTS AND DISCUSSION

As a result of monitoring during the rainy season in 2019, it was possible to obtain a number of observations at the Reotala site showing that, before the occurrence of slope failures, the tilting angle gradually increased with rainfall and then resulted in slope collapse. The trend of the tilting angle before the slope failure at R3 and R4 (figure 44), and 1-hour rainfall and accumulated rainfall at that time, are shown as examples in figures 45 and 46. The 1-hour rainfall indicates the amount of rainfall that occurred one hour immediately before a certain time. The accumulated rainfall indicates the total amount of rainfall since the rain began. If no rainfall has been observed for 12 consecutive hours, the accumulated rainfall is reset to 0 millimeters. The explanation of the graphs shown in figures 45 and 46 and the results are described below.

date and time. Assuming that the changes in tilt angle are a function of mass movement, it is thought that this result indicates that mass movement started at 1:40 on July 7, then stopped once and, after that, mass movement started again at 20:20 on July 7. After that, since data were no longer acquired after 3:20 on July 8, it was judged that the slope tilt sensor was broken because of slope failure, and data could not be acquired. Therefore, the timing of the slope failure is inferred to have been at 3:10 on July 8.

Figure 45B shows the 1-hour rainfall and accumulated rainfall on the vertical axis, and the horizontal axis shows the same date and time as figure 45A. As a result of the observation, the accumulated rainfall (117.5 millimeters) at 3:10 on July 8, which was considered to have caused the slope failure, and the 1-hour rainfall at 3:00 on July 8 immediately before the slope failure was 10.0 millimeters/hour. Also, it can be seen that at the time of the start of

Figure 45A shows the tilting angle on the vertical axis of the slope tilt sensor R3, and the horizontal axis shows the

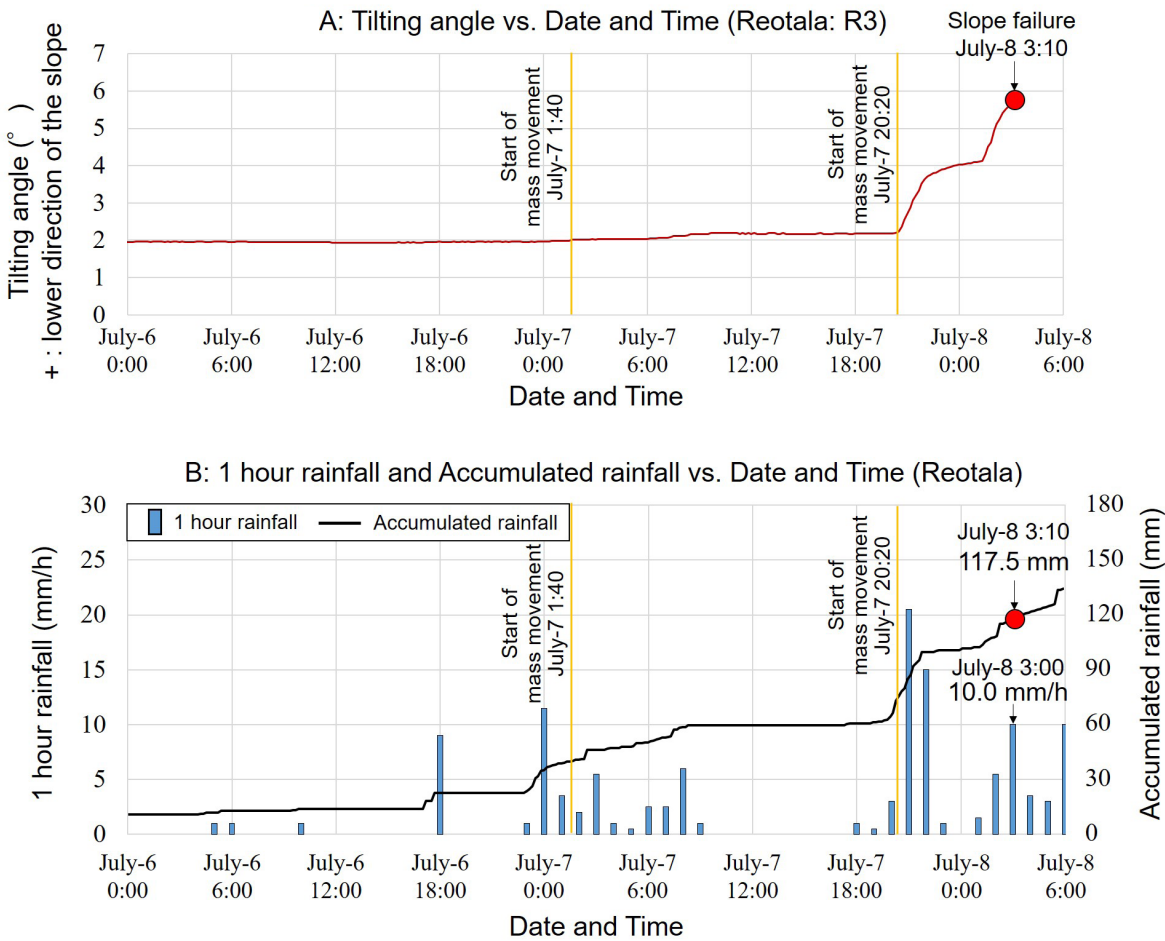


Figure 45: Rain gauge and slope tilt sensor data from R3 site at Reotala

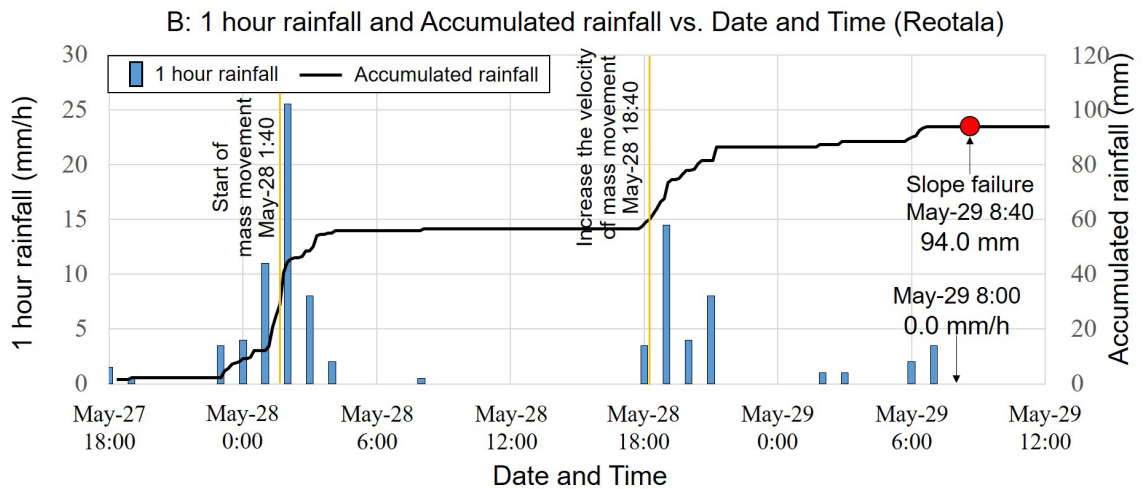
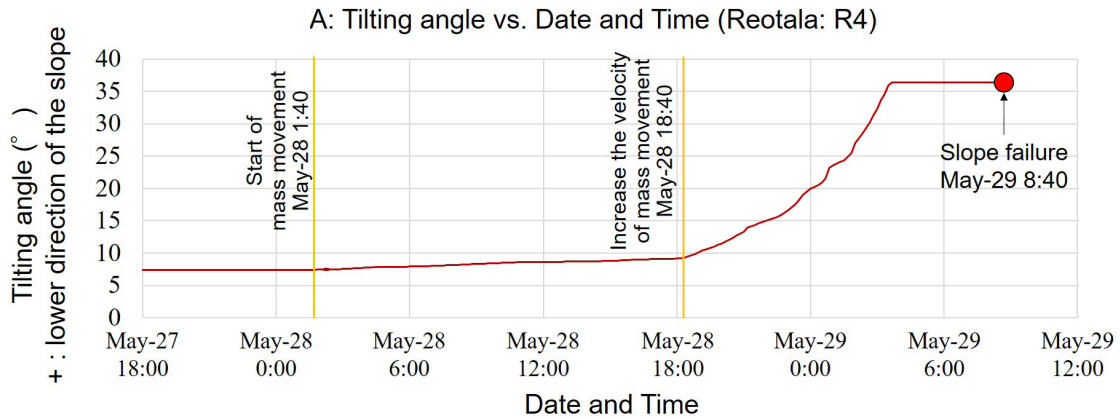


Figure 46:  
Rain gauge and slope tilt sensor data from R4 site at Reotala

the mass movement shown in figure 45A, the accumulated rainfall had increased.

In figure 46A, the vertical axis shows the tilting angle of the slope tilt sensor at R4, and the horizontal axis shows the date and time. This result indicates that mass movement started at 1:40 on May 28 and that the tilting angle rapidly increased from 18:40 on May 28. The slope failure was observed at 8:40 on May 29.

In figure 46B, the vertical axis shows the 1-hour rainfall and accumulated rainfall, and the horizontal axis shows the same date and time as figure 46A. As a result of the observation, the accumulated rainfall at 8:40 on May 29, which was thought to have caused the slope failure, was 94.0 millimeters, and the 1-hour rainfall at 8:00 on May 29 immediately before the slope failure was 0.0 millimeters/hour. In addition, it can be seen that, at the time of the start and increase in the velocity of the mass movement shown in figure 46A, the accumulated rainfall had increased.

It is observed that the tilting angle of the slope surface increases at an accelerated rate as a precursor phenomenon before slope failure occurs (Saito 1960). From the results shown in figure 45A and figure 46A, it is thought that the slope tilt sensor succeeded in observing the timing of slope failure occurrence and its precursors, which are mass movements. Besides, from the results of figures 45B and 46B, it is inferred that the rainfall caused the start of mass movement or an increase in the velocity of the mass movement. However, concerning the setting of the rainfall thresholds for ex ante traffic control, it is difficult to determine from just two cases, R3 and R4, whether lower accumulated rainfall or 1-hour rainfall also needs to be considered.

## 6.4 SUMMARY AND FUTURE PLAN

In selecting pilot sites for slope monitoring, the JICA Project utilized the results of satellite monitoring implemented by the WB Project, which conducted macro-scale slope monitoring away from the sites. Slope monitoring for ex ante traffic control—the first attempt in Bhutan at the selected pilot sites—has been carried out since April 2019; these sites continue to be monitored. As a result of slope monitoring during the rainy season in 2019, multiple slope tilt sensors successfully monitored the precursors and the timings of the occurrence of slope failures, demonstrating that the results of the monitoring of the WB Project could be fully utilized even in the micro-scale work on site.

Slope monitoring using the automated rain gauges and the slope tilt sensors will be implemented continuously to set and review the rainfall thresholds for ex ante traffic control. In January 2021, the accumulated monitoring data will be analyzed and evaluated, and the first rainfall thresholds for ex ante traffic control will be determined. From February 2021 to March 2021, drills will be conducted on ex ante traffic control from February to March 2021 to start the operation of ex ante traffic control based on rainfall in Bhutan from July 2021. Moreover, a system will be established with the objective in which the DoR can take the initiative and mainly perform the necessary procedures by themselves, from issuing warnings to implementing roadblocks.

**AS A RESULT OF SLOPE MONITORING DURING THE RAINY SEASON IN 2019, MULTIPLE SLOPE TILT SENSORS SUCCESSFULLY MONITORED THE PRECURSORS AND THE TIMINGS OF THE OCCURRENCE OF SLOPE FAILURES, DEMONSTRATING THAT THE RESULTS OF THE MONITORING OF THE WB PROJECT COULD BE FULLY UTILIZED EVEN IN THE MICRO-SCALE WORK ON SITE.**

---

## DATA PRESENTATION AND SHARING PLATFORMS

---

07

The analysis of interferometric synthetic aperture radar (InSAR) data produced a series of products, some of which can be considered intermediate products and some of which can be regarded as final products that can be used by an end-user (Department of Transportation, Disaster Management agency, etc.). The useful products of interest are listed and described in this section and are available online.

### 7.1 GIS FILES: ESRI SHAPEFILES AND GOOGLE EARTH .KMZ FILES

The primary output of the persistent scatterers (PS) InSAR analysis is the set of PS points containing information on their displacement through time, the calculated velocity (from linear regression of displacement vs. time), the InSAR processing coherence, and some other output parameters from the processing that are not discussed here. This output is given in an electronic file in the ESRI shapefile (.shp) format to be used in a geographic information system (GIS) platform (e.g., ArcMap, QGIS, etc.). Additional processing of this dataset produced the 95th percentile velocity and coherence filtered dataset, from which the clustering analysis further produced the point cluster datasets. This cluster dataset was further processed to compute the hazard score and the exposure score for each point cluster, and from that, the risk score and ranking was obtained.

This information was then incorporated into the dataset, and this dataset can be considered the final analysis product in GIS format, which we have kept in the original ESRI shapefile format. One shapefile was produced for each of the three sites. The attribute table for these files contains the following information for each PS point: a field named "Vel\_mm\_y," which contains the displacement velocity. A field named "Coherence," which contains the coherence values for each PS point. A series of fields with names that start with the "D\_" characters and are followed by the date in the format YYYYMMDD, where YYYY is the year in four-digit format (e.g., 2018), MM is the month in two-digit format (e.g., 01 for January), and DD is the day in two-digit format (e.g., 07 for the seventh day in a month), which contain the

cumulative displacement values for each PS point, starting from the date of the first SAR image used for the analysis (the displacement for that images is always equal to zero). A field named "cluster," which contains the cluster values to which each PS point belongs. A field named "risk\_score," which includes the combined risk scores for each PS point, as defined from this document and the accompanying Excel spreadsheet data. And a field named "risk\_rank," which contains the ranking, from the largest to the smallest risk score, for all the clusters.

### 7.2 ARCGIS ONLINE WEBMAPS

In addition to the GIS files provided as electronic appendixes and in the online Google Drive repository, we have also created three ArcGIS online webmaps, one for each test site, that allow the users to interactively visualize maps with the GIS data without the need of a separate GIS platform: only a web browser and access to the internet is required to access these files.

The map contents are explained in an accompanying ASCII text (.txt) file also included in the online Google Drive repository, but for the most part, the maps should be self-explanatory.

Links to the maps can be accessed here:

Site 1 (India): <https://arcg.is/uOyr1>

Site 2 (Bhutan): <https://arcg.is/1G8emG>

Site 3 (Nepal): <https://arcg.is/rrLqy>

## GENERAL DISCUSSION AND CONCLUSIONS

08

### 8.1 PS INSAR DATA GENERATION AND INTERPRETATION WITHIN THE CONTEXT OF SLOPE STABILITY AND LANDSLIDES

The persistent scatterers interferometric synthetic aperture radar (PS InSAR) analysis undertaken for the three test sites shows a wide range of displacement behaviors.

The processing at each site gave a large number of PS points—on the order of hundreds of thousands to more than a million. Extracting useful information from such vast datasets requires careful consideration of the goals of the project, the possible products that can be generated, and the analysis necessary to make these products.

Using the InSAR method it is likely to reflect the real ground surface displacement and velocities with substantial confidence. The primary measure of data quality is the coherence value, also reported as an output by the processing software. Based on these values, it is possible to select the highest-quality data points, which guarantees that the InSAR output is most likely to reflect real ground surface displacements and velocities. Because of the relative or comparative nature of our analysis (i.e., we find and identify the locations more likely to have unstable slopes and to have produced landslides) we chose a statistical criterion to select only the data with the best quality—that is, those data points with a coherence above the 95th percentile for the whole dataset at each site. Such a filtering criterion allowed us to select only the data points most likely to show real ground displacement. At this time, it is essential to clarify that such displacements would not necessarily reflect a broader behavior of the slope in a geological or geotechnical context and would warrant further considerations of the significance of these measured displacements.

Even though a premise driving our analysis is that displacement and velocity correlate inversely with slope stability (i.e., the more displacement/velocity, the less

stable the slope), it is important to recognize that the highest amount of displacement or velocity does not necessarily imply that the particular slope will become unstable and produce landslides. The ground displacement and velocity measurements can have a complex and not always straightforward relationship to the potential for slope instability and land sliding. The opposite is also true: the absence of measured displacement or a low velocity does not guarantee that the slope will be stable in the long run. Considering geological, geotechnical, and other technical criteria are necessary to draw conclusions from the data and provide a contextualized and more sound interpretation of the measured displacement fields. In our analysis, we have attempted to include many of those criteria as possible to make a broad analysis of the hazard implications of such displacements by considering other independent criteria—such as slope inclination and spatial and velocity clustering.

Our findings indicate that the vast majority of those points showed relatively low displacements over time (e.g., velocities < 5 millimeters/year); for such low values, distinguishing between real ground movements from random and spuriously induced values (i.e., the signal vs. the noise) can be very difficult. Such low-velocity values are also less relevant for the slope stability problem that we are analyzing, under the assumption that higher displacements and velocities are correlated with less stable slopes. This leads to the consideration of focusing our analysis on the higher velocities (velocities above the 95th percentile for each site). This is a rather high value to use as a cutoff, the process generated a large enough set of points to review (given the vast amount of data). It is, however, essential to recognize that points with lower velocities may also be associated with slope instabilities in the future. If an area was to show possible signs of slope instability in the field (e.g., ground cracking and deformation) but was not included in our selection of points above the 95th percentile of velocities, such a location should be assessed for potential slope instability and landslide hazards and monitored accordingly.

Due to image decoherence, the InSAR technique would not work effectively in terrain areas moving at high velocities (> 25 millimeters/year). Therefore, such an approach was

also applied to locations for which we did not obtain even a single PS point.. Such cases, however, may be more likely to be identified and noticed in the field, as large deformations may cause more visible signs (e.g., ground cracking, structural damage, infrastructure deformation, smaller subsidiary slides, etc.) related to the movement and potential slope instability.

Further, clustering such points based on proximity and velocity is an effective criterion used for identifying potentially unstable slopes. From a slope instability and landslide hazard perspective, it is also important to consider the slope as a finite geotechnical entity that extends over some area. An unstable slope that is moving and may collapse to form a landslide may tend to show a coherent pattern of movement over the extent of the area becoming unstable—that is, all the points in that area may be moving in a similar direction, and they may tend to move at a similar velocity. This consideration allowed us to establish our second criterion for identifying points that could be relevant to the slope instability and landslide hazard problem: points that are close in space and are moving in the same direction and similar velocities are more likely to reflect an unstable slope.

To analyze individual points, it is important to note that the absence of clustering does not necessarily imply the absence of unstable slopes, and that any other indication in the field that a slope may become unstable should not be ignored. The clustering criterion is used only to assess what areas are more likely to become unstable but does not exclude all other regions that do not exhibit clusters from such consideration. The clustering analysis then allows us to focus on broader slope areas that, on the whole, show relatively high displacement velocities over a given number of points, with a consistent pattern of direction and velocity, and that have already been selected from the InSAR dataset because of their high quality (coherence values). It is with this dataset that we do the hazard, exposure, and risk scoring and ranking analysis.

## **8.2 TRANSLATING INSAR DISPLACEMENT AND VELOCITIES INTO A MEASURE OF HAZARD AND COMBINING IT WITH EXPOSURE INFORMATION TO PROVIDE A FIRST-ORDER RISK ESTIMATION**

One of the major goals of our project is to produce a landslide risk prioritization of sites indicating specific landslides that have the highest risk to roads and buildings. Prioritization of the sites allows for effective hazard planning that can be utilized by relevant agencies and policy makers to make crucial decisions. Further, the relative risk ranking may provide not only a way to prioritize sites for risk mitigation but this information can be utilized for timely interventions as well.

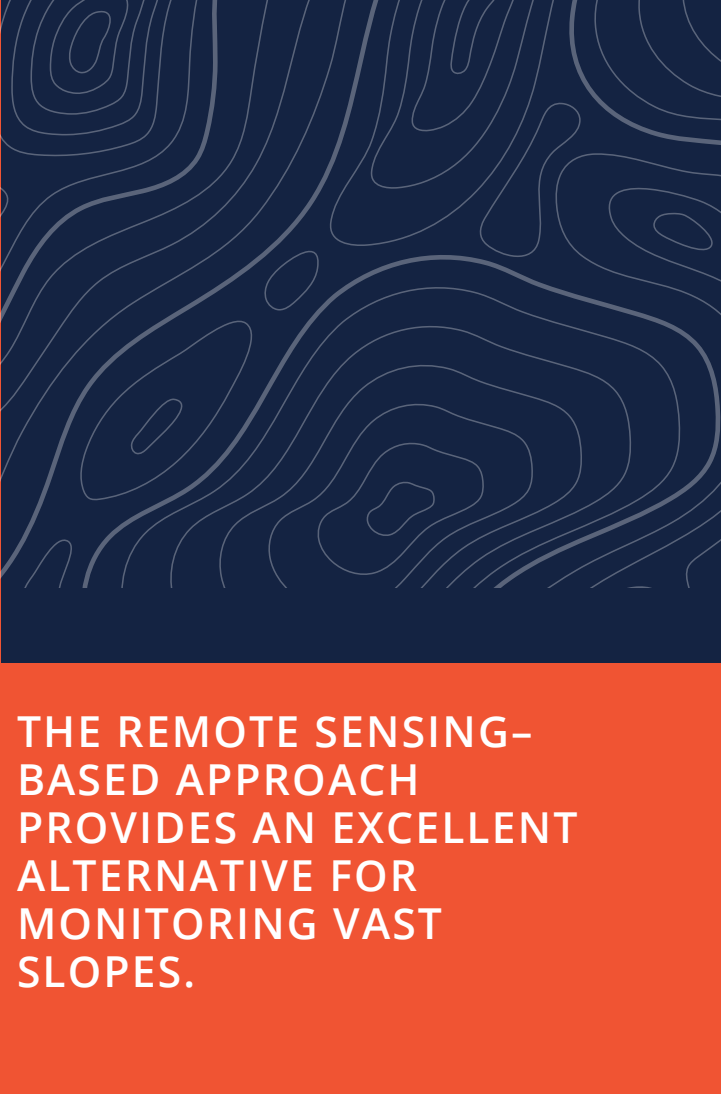
The terrain displacement and velocity information were extracted from the PS InSAR analysis, which was further refined by coherence filtering, velocity filtering, and clustering analysis, which together do not provide a hazard estimation by themselves. Ideally, this information would be used in a physically based geotechnical slope stability model that would allow us to estimate a factor of safety of the slope or some other similar metric aimed at assessing how stable or unstable the slope is. However, such a modeling effort would require a vast amount of data on the slope material properties and slope conditions (e.g., water table depth, etc.) at each of the points under consideration, a task that was beyond the scope of this project. Instead, we used a somewhat subjective, weighting-based hazard-scoring method. Although the process is subjective and relies on the weight given by the expert to the different hazard variable categories, the methodology is transparent and open to modifications by the user, should they have different criteria to weight the different input variables.

But hazard alone does not present the full picture of the problem; it is the risk, the interaction of the hazard

with some form of vulnerability, that is the core of the problem of landslide losses. The vulnerability can be conceived of as a very complex set of characteristics of the system that is exposed to losses as a result of a hazard, and, therefore, to characterize the detailed vulnerability, it would also be necessary to assess a multi-dimensional set of variables, including socioeconomic and physical characteristics of the exposed population and infrastructure. As with the hazard, such an undertaking would be beyond the scope of the project, but to generate actionable insights from our analysis we used a similar subjective weighting-based method to determine risk. We also chose to consider only one aspect of vulnerability, perhaps the most obvious one: physical exposure. Although physical exposure is a necessary condition, it is not a sufficient one, as proximity does not imply vulnerability. Still, it is perhaps the most important variable in many cases of landslides, and it is also one of the easiest to assess. This led us to consider exposure as our proxy for vulnerability and to perform our scoring analysis. The combination of the hazard and exposure scores into a risk score allows us to do a relative ranking of the point clusters based on the risk scores. This is the final aim of the project: to produce a landslide risk prioritization of sites indicating which landslide has the highest risk to roads and buildings. This is the main product, provided as a series of GIS files with those cluster priority data.

In conclusion, our analysis shows a large number of locations where potential ground displacement could be related to slope instability at three testing sites in India, Bhutan, and Nepal. Further refinement and filtering of the data, considering the data coherence and minimum velocities, isolate only those points that are more likely to show terrain displacement that could be significant for slope stability and landslide hazard assessment purposes. A subset of the points is then selected to also include the spatial geo-technical context as a criterion in our analysis of the hazard.

Based on an additional assessment of houses/buildings and road exposure and on the velocity and slope characteristics of the point clusters, a weight-based scoring method is applied to assign hazard and exposure score to all the clusters. From that estimate, a combined risk score is obtained. From the relative ordering of the risk scores (largest to smallest), a risk ranking is achieved. The hazard scores strongly influence risks ranking, but exposure also plays a key role, highlighting the important fact that risk is not simply equal to hazard. The relative risk ranking may provide a way to prioritize site selection for risk mitigation or other intervention purposes.



**THE REMOTE SENSING-BASED APPROACH PROVIDES AN EXCELLENT ALTERNATIVE FOR MONITORING VAST SLOPES.**

### **8.3 SYSTEM SETUP AND WORK FLOW**

This report highlights the application of satellite-based SAR data and in situ measurements for slope stability monitoring. Implementing the SAR-based monitoring system, requires inhouse capability for image processing with SAR processing software. Relevant agencies involved in hazard planning can outsource SAR data processing to consulting firms and universities. In case in-house capabilities are not sufficient. Several SAR satellites are available for data acquisition through the European, Canadian, German, and Japanese space agencies. While some of these data sources are paid, many others are available free of cost. An important SAR dataset that is available for free is the Sentinel data from the European Space Agency. Typically, 15-20 images from a site are required to perform PSInSAR. The processing of the SAR images needs high-end computing capability. The SAR image processing involves a line-of-sight measurement of displacement over time. In situ measurements (rain gauge and slope tilt sensors), as discussed in chapter 6, can be used to verify or to compliment the SAR-based displacement measurements. The rain gauge can help confirm whether rainfall is the trigger for the slope movement.



## 8.4 BENEFITS OF INSAR AND *IN SITU*-BASED SLOPE MONITORING

The InSAR-based approach provides an all-weather and all-day monitoring solution for landslide hazards. The remote sensing-based approach provides an excellent alternative for hazard planning agencies, and policy makers to monitor vast slopes in mountainous areas that are faced with issues such as access, lack of power for instrumentation, vandalism of instruments in remote locations, and so on. As climate change affects communities through the likely increase in weather- and climate-related hazards such as landslides, development activities need careful monitoring for disaster risk reduction. Development activities in mountainous terrains are highly vulnerable to landslide hazards. In-situ monitoring of landslide hazards in these mountainous areas can be challenging because of the vastness of the asset that needs to be monitored (e.g., all along the road corridors), access issues, lack of power for instrumentation, vandalism of instruments in remote locations, and so on. The remote sensing-based approach provides an excellent alternative for monitoring vast slopes. Notably, the InSAR-based approach provides an all-weather and all-day monitoring solution for landslide hazards. The InSAR images can be used to detect millimeter-scale ground movements, which could indicate early signs of landslide hazards. The limitation of the InSAR-based approach is that, in highly vegetated areas, the increased noise could impact the data. In summary, the InSAR-based remote-sensing approach can be extremely valuable in screening large areas for landslide hazards.

In highly vegetated areas, the increased noise can impact the data, which is a limitation of the InSAR-based approach. However, even with its limitations, the InSAR-based remote-sensing approach can be extremely valuable tool in screening large areas for landslide hazards. Our case studies indicate that, the PS point densities are commonly tens to hundreds of points per square kilometer. The cost to acquire and process InSAR-based PS points ranges from US\$2 to US\$20/ point compared to in situ instrumentation that would cost US\$1,500 to US\$6,000/point (Escobar-Wolf et al. 2015; Yang et al. 2017). Considering the cost of InSAR and in situ-based slope monitoring, the InSAR-based method can be a cost-effective approach for screening large area.

To achieve a more focused, data-driven disaster risk reduction, the in situ monitoring can be employed once an area

is screened for landslide hazard, and particularly for the critical slopes that show signs of distress as detected from the remote sensing. The advantage of in situ monitoring is that it provides much higher temporal resolution (minute-to-minute detection of movements) compared to satellite-based InSAR monitoring (weekly to biweekly monitoring). Further, by acquiring a high temporal resolution early warning systems can be developed to notify communities before a landslide occurs, making the satellite-based InSAR monitoring and in situ measurements are complementary technologies that can be used for landslide disaster risk reduction.

## 8.5 CHALLENGES AND LESSONS

This report demonstrates the promise of the PSI approach for slope displacement monitoring and the complementary nature of in situ monitoring. The PSI technique allows measuring displacements on the order of just a few millimeters for a point on the ground that consistently scatters the radar signal back to the satellite. For those persistent scatterers, it is possible to achieve precision; the number of persistent scatterers that can be effectively measured depends on the terrain conditions (e.g., how much vegetation and how many human-built structures there are). Even though the methodology is very precise, several important limitations must be considered, mainly related to how much the terrain may have been displaced between two InSAR image acquisitions. When the displacement is too large, the images cannot be correlated, and displacement cannot be calculated. In other words, if the displacement between two InSAR images is more than half the wavelength, or a few to 10 centimeters depending on the band type, then such displacements cannot be measured using PSI. Therefore, a very fast-moving slope movement or landslides may not be suitable for monitoring with InSAR, but such landslides are more likely to be identified through other means (e.g., field observations) because they will be much more noticeable (e.g., through the crack formation and structure deformation).

One of the significant lessons learned from this project is that the PSI approach can be valuable for evaluating a large landslide-prone area for planning new infrastructure or monitoring existing infrastructure. When a region is monitored using PSI, it is not possible to know upfront where the persistent scatterer points will be obtained. This can be a challenge when a specific location needs to be monitored. However, when PSI processing is completed, we often get a large number of persistent scatterer points in an image scene, which makes it highly likely that you would have points on locations of interest or in its vicinity. Another challenge is that in heavily vegetated areas, the persistent scatterer points density can be significantly reduced.

## 8.6 FUTURE OPPORTUNITIES

Remote sensing shows excellent promise in monitoring Earth surface processes using different wavelengths of the electromagnetic spectrum at a very high temporal resolution. The radar wavelength is valuable to measure ground displacement. As this project shows, utilizing multiple radar images (using the persistent scatterer interferometry, or PSI), we can measure millimeter-scale displacements on the ground. Often, measuring the displacements/movements on the Earth's surface can indicate sub-surficial or surficial processes that could lead to a vulnerability or disaster. Previous projects have also shown that monitoring geohazards—such as landslides, ground subsidence, earthquakes, and volcanic processes—as well as monitoring the stability of critical infrastructure such as bridges, dams, tunnels, and so on can be accomplished by measuring ground displacements (DePrekel, Bouali, and Oommen 2018; Oommen Bouali, and Wolf 2019). The following list identifies some of the future opportunities for this technique in the development sector.



**Planning and Policy.** The PSI-based analysis can aid in cases where the historical record of vulnerabilities is limited or sparse. Land use planning and policy development need an understanding of the vulnerabilities within the region of interest. Often, documentation of these vulnerabilities is not available in developing countries. In such situations, planning and policy decisions have to be made with limited or no data. The PSI-based analysis could aid in such cases where the historical record of vulnerabilities is limited or sparse. The availability of historical archives of radar data provides the opportunity to analyze how the region of interest has performed in the past. This allows policy makers to identify areas within the region that are vulnerable to land sliding or subsidence and make an informed decision for planning and policy development. Such informed planning and policy development can lead to significant risk reduction, cost savings, and safer communities.



**Infrastructure Routing.** Understanding the vulnerabilities at the site is essential for planning the route of a transport corridor or locating the site of critical infrastructure. The vulnerability assessment is often accomplished by modeling the hazards. The PSI-based analysis could complement the hazard analysis by providing a perspective on how the vulnerabilities have performed over time. This information could be valuable in deciding between alternate routes or multiple sites. Such decisions can have long-term implications in terms of the maintenance cost, safety, and sustainability of the infrastructure.



**Infrastructure Monitoring.** Aging infrastructure and extreme weather events are straining our infrastructure globally. This strain calls for improved monitoring of our infrastructure to ensure safety and security. The traditional approach of in-situ monitoring can be tedious and costly. This approach could also lack the spatial resolution to monitor massive infrastructure. The PSI-based analysis could provide a valuable alternative to monitor the condition of infrastructure and alert communities that are within the zone of risk in the case of any unusual activity. These alerts could also be valuable in implementing corrective measures before the conditions at a site become dangerous.



**Prioritizing Hazard Mitigation.** Mitigating geohazards is important for the safety of infrastructure. However, limited resources require prioritizing mitigation activities. In some cases, these priorities are evident because of visible damage or destruction from the geohazard, but in some other cases, it may not be so apparent. In such situations, the PSI-based ground displacement measure can help to proactively identify the sites that need to be mitigated or prioritized for mitigation. The rate of displacement at a site can indicate how vulnerable that site is and enable it to rank the sites.



**Past Failure Investigation.** Understanding past failures can be important to ensure those mistakes are not repeated. The PSI-based method can be used to investigate the causes of failure of infrastructure or a site. Particularly, a forensic investigation can be carried out to identify when the displacements begin at a site. Knowing the time when it started and at what rate it progressed can hint to the processes occurring in the region and identify the factors that influenced the failure to occur.



**Countrywide or Regionwide Hazard Monitoring.** Large-scale monitoring of geohazards (countrywide and at the regional scale) is becoming more prevalent and accessible as the satellite-based radar data become freely available. Currently, Norway is doing countrywide PSI monitoring of landslides. Such an approach can be valuable for countries or regions that are highly vulnerable to landslides and other ground displacement hazards. It can also be used for large-scale asset management.



---

REFERENCES  
& APPENDIX

---

# REFERENCES

- BBS. 2013. "Heavy Rainfall Causes Landslides." *BBS*, July 8, 2013. <http://www.bbs.bt/news/?p=29194>.
- BBS. 2015. "MoWHS to Take Up Major Mitigation of Reotala Slide." *BBS*, September 14, 2015. <http://www.bbs.bt/news/?p=53256>.
- BBS. 2016. "Bhutan Still Following India's Standards to Counter Road Slope Disasters." *BBS*, June 14, 2016. <http://www.bbs.bt/news/?p=59967>.
- BBS. 2017. "Heavy Downpour Disrupts Road Networks across the Country." *BBS*, July 11, 2017. <http://www.bbs.bt/news/?p=75839>.
- Bhambri, R., M. Mehta, D. P. Dobhal, A. K. Gupta, B. Pratap, K. Kesarwani, and A. Verma. 2016. "Devastation in the Kedarnath (Mandakini) Valley, Garhwal Himalaya, during 16–17 June 2013: A Remote Sensing and Ground-Based Assessment." *Natural Hazards* 80 (3):1801–22.
- Bianchini, S., A. Ciampalini, F. Raspini, F. Bardi, F. Di Traglia, S. Moretti, and N. Casagli. 2015. "Multi-Temporal Evaluation of Landslide Movements and Impacts on Buildings in San Fratello (Italy) by Means of C-Band and X-Band PSI Data." *Pure and Applied Geophysics* 172 (11): 3043–65.
- Bist, K. S. and M. P. Sah. 1999. "The Devastating Landslide of August 1998 in Ukhimath Area, Rudraprayag District, Garhwal Himalaya." *Current Science* 76 (4): 481–84.
- Bouali, E. H., T. Oommen, and R. Escobar-Wolf. 2016. Interferometric Stacking Toward Geohazard Identification and Geotechnical Asset Monitoring." *Infrastructure Systems* 22 (2): 05016001.
- Bouali, E. H., T. Oommen, and R. Escobar-Wolf. 2018. "Mapping of Slow Landslides on the Palos Verdes Peninsula Using the California Landslide Inventory and Persistent Scatterer Interferometry." *Landslides* 15 (3): 439–52.
- Corominas, J., C. van Westen, P. Frattini, L. Cascini, J.-P. Malet, S. Fotopoulou, F. Catani, M. Van Den Eeckhaut, O. Mavrouli, F. Agliardi, K. Pitilakis, M. G. Winter, M. Pastor, S. Ferlisi, V. Tofani, J. Hervás, and J. T. Smith. 2014. "Recommendations for the Quantitative Analysis of Landslide Risk." *Bulletin of Engineering Geology and the Environment* 73.2 (2014): 209–63.
- DePrekel, K., E. Bouali, and T. Oommen. 2018. "Monitoring the Impact of Groundwater Pumping on Infrastructure Using Geographic Information System (GIS) and Persistent Scatterer Interferometry (PSI)." *Infrastructures* 3 (4): 57.
- ESA. 2019. User Guides – Sentinel-1 SAR – Acquisition Modes. *ESA Sentinel Online*. <https://sentinel.esa.int/web/sentinel/user-guides/sentinel-1-sar/acquisition-modes>.
- Fell, R., J. Corominas, C. Bonnard, L. Cascini, E. Leroi, and W. Savage. 2008. "Guidelines for Landslide Susceptibility, Hazard and Risk Zoning for Land-Use Planning. Comment." *Engineering Geology* 102.3 (2008): 99–111.
- Ferretti, A., C. Prati, and F. Rocca. 2000. "Nonlinear Subsidence Rate Estimation Using Permanent Scatterers in Differential SAR Interferometry." *IEEE Transactions on Geosciences and Remote Sensing* 38 (5): 2202–12.
- Ferretti, A., C. Prati, and F. Rocca. 2001. "Permanent Scatterers in SAR Interferometry." *IEEE Transactions on Geosciences and Remote Sensing* 39 (1): 8–20.
- Gupta, V., R. K. Bhasin, A. M. Kaynia, R. S. Tandon, and B. Venkateshwarlu. 2016. "Landslide Hazard in the Nainital Township, Kumaun Himalaya, India: The Case of September 2014 Balia Nala Landslide." *Natural Hazards* 80 (2): 863–77.
- Highland, L. and P. T. Bobrowsky. 2008. *The Landslide Handbook: A Guide to Understanding Landslides*. Reston: US Geological Survey.
- The Himalayan Times. 2009. "Highways Disrupted, Man Missing." The Himalayan Times, October 7, 2009. <https://thehimalayantimes.com/news-archives/latest/highways-disrupted-man-missing/>.
- Islam, M. A., S. L. Chatteraj, and C. P. Ray. 2014. "Ukhimath Landslide 2012 at Uttarakhand, India: Causes and Consequences." *International Journal of Geomatics and Geosciences* 4 (3): 544.
- Jagran Post. 2014. "Kedarnath Yatra Hit by Landslides." *Jagran Post*, <http://post.jagran.com/kedarnath-yatra-hit-by-landslides-1400928358>.
- The Kathmandu Post. 2013. "Landslide Obstructs Transportation along Rapti Highway." *The Kathmandu Post*, October 9, 2013. <http://kathmandupost.ekantipur.com/news/2013-10-09/landslide-obstructs-transportation-along-rapti-highway.html>.
- The Kathmandu Post. 2018. "75 Houses in Khalanga Town Face Danger from Landslides." *The Kathmandu Post*, August 7, 2018. <http://kathmandupost.ekantipur.com/printedition/news/2018-08-07/75-houses-in-khalanga-town-face-danger-from-landslides.html>.
- Klose, M., B. Damm, and B. Terhorst. 2015. "Landslide Cost Modeling for Transportation Infrastructures: A Methodological Approach." *Landslides* 12 (2): 321–34.
- KuenselOnline. 2015. "Heavy Rains Cause Several Landslides Nationwide." *KuenselOnline*, September 5, 2015. <http://www.kuenselonline.com/heavy-rains-cause-several-landslides-nationwide/>.
- KuenselOnline. 2016. "Reotala Bailey Bridge Still Closed to Traffic." *KuenselOnline*,

- November 15, 2016. <http://www.kuenselonline.com/reotala-bridge-repaired-open-to-traffic/>
- KuenselOnline. 2017. Roadblocks close six highways. *KuenselOnline*, July 11, 2107. <http://www.kuenselonline.com/roadblocks-close-six-highways/>
- KuenselOnline. 2018. "Several Blocks Open to Traffic across the Country." *KuenselOnline*, August 4, 2018. <http://www.kuenselonline.com/several-blocks-open-to-traffic-across-the-country/>
- Ministry of Land, Infrastructure, Transport and Tourism Road Bureau National Road Division Planning Specialist. 2002. "Immediate Operation Related to Relaxation of Pre-Traffic Regulation" (Japanese).
- Ministry of Land, Infrastructure, Transport and Tourism. 2019. "Ex-Ante Traffic Control" (Japanese). <https://www.mlit.go.jp/road/bosai/jizenkisei/kisei.html>.
- Nepal Monitor. 2014. "Landslides Kill One in Rukum, Two in Rolpa." *Nepal Monitor*, August 14, 2014. <https://nepalmonitor.org/reports/view/3729>.
- Oommen, T. 2019. *Proactive Monitoring and Assessment of Critical Slopes Using Remote Sensing in the Transport Sector, South Asia*. World Bank Project Final Report, 39–50.
- Oommen, T., E. H. Bouali, and R. E. Wolf. 2019. "New Paradigm in Geotechnical Performance Monitoring Using Remote Sensing." In *Geotechnical Design and Practice*, edited by K. Ilamparuthi and R. G. Robinson, 195–201. Developments in Geotechnical Engineering book series. Singapore: Springer.
- Reliefweb. 2018. "75 Houses in Khalanga Town Face Danger from Landslides." *Reliefweb*, August 7, 2018. <https://reliefweb.int/report/nepal/75-houses-khalanga-town-face-danger-landslides>.
- Rosi, A., V. Tofani, L. Tanteri, C. Tacconi Stefanelli, A. Agostini, F. Catani, and N. Casagli. 2018. "The New Landslide Inventory of Tuscany (Italy) Updated with PS-InSAR: Geomorphological Features and Landslide Distribution." *Landslides* 15 (1): 5–19.
- Saito, M. 1960. "Slope Failure and Strain Measurement" (Japanese). *Japanese Society of Soil Mechanics and Foundation Engineering, Special Issue on Soil and Basics*, Vol. 1: "In Situ Test and Measurement Methods," 22–33.
- Sarmap (2017) SARscape v. 5.2 software.
- Shigeki, K. and M. Toshimi. 2006. "Practical Methods Using Interferometric SAR for Subtle Land Surface Monitoring." (Japanese). *Proceedings of Applied Computing in Civil Engineering, Japan Society of Civil Engineers* 31: 45–8.
- Times of India. 2017. "Landslide Blocks NH Traffic for Hours in Rudraprayag District." *Times of India*, June 29, 2017. <https://timesofindia.indiatimes.com/city/dehradun/landslide-blocks-nh-traffic-for-hours-in-rudraprayag-district/articleshow/59825641.cms>
- Upreti, B. N. and M. R. Dhital. 1996. "Landslide Studies in Nepal." Kathmandu: International Centre for Integrated Mountain Development (ICIMD).
- West Nippon Expressway Cooperation Limited, Chugoku Branch. 2015. *Disaster Prevention Work Implementation Rules* (Japanese), 57.
- Winter, M. G., B. Shearer, D. Palmer, D. Peeling, C. Harmer, and J. Sharpe. 2016. "The Economic Impact of Landslides and Floods on the Road Network." *Procedia Engineering* 143: 1425–34.
- Xue, Y. T., X. M. Meng, K. Li, and G. Chen. 2015. "Loess Slope Instability Assessment Based on PS-InSAR Detected and Spatial Analysis in Lanzhou Region, China." *Advanced Materials Research* 1065: 2342–52.

# APPENDIX



## **APPENDIX. KEY QUESTIONS AND ANSWERS FROM THE ONLINE WEBEX PRESENTATION TO THE NEPAL AND BHUTAN TEAMS ON APRIL 3, 2019**

An online presentation was given on April 3, 2019, by the Michigan Technological University Team. The audience included the Nepal and Bhutan technical teams. The presentation lasted 2 hours. Following is a summary of the main topics raised after the presentation during the questions and answers that followed.

### **A.1 PRECISION OF THE MEASUREMENTS AND LIMITATIONS OF THE METHOD**

Some of the questions asked by the audience touched on the issue of measurement precision: how precise are the displacement and velocity measurements of the ground? As explained after the presentation, the PS InSAR technique allows measuring displacements on the order of just a few millimeters for a point on the ground that consistently scatters the radar signal back to the satellite. For those persistent scatterers, it is possible to achieve such precision; how many of those persistent scatterers can be measured depends on the terrain conditions (e.g., how much vegetation and how many human-built structures there are). Although the method can be very precise, several important limitations must be considered, mainly related to how much the terrain may have been displaced between two InSAR image acquisitions. When the displacement is too large, the images cannot be correlated



and displacement cannot be calculated. Therefore, very fast moving landslides may not be suitable for monitoring with InSAR, but such landslides are more likely to be identified through other means (e.g., field observations) because they will be much more noticeable (e.g., through crack formation and structure deformation).

## **A.2 RESOLUTION TO MEASURE DISPLACEMENTS AND VELOCITIES**

Although related to the previous discussion, the question is: what is the spatial resolution of the displacement and velocity information that can be retrieved from the InSAR technique? Although the original data from Sentinel 1 will have a spatial resolution of ~ 20 meters (pixel size), the persistent scatterer technique relies on finding points (pixels) for which the signal is persistently scattered (in a similar way) repeatedly over many image acquisitions, and the density of such points can vary considerably depending on the terrain conditions. Over heavily forested areas, the point density will be very low, but over non-vegetated or human structure-covered areas, the density can be very high. Many active landslides show low vegetation coverage as a result of the landslide movement, and sometimes this is an advantage from the perspective of using the PS InSAR technique. The clustering processing also tries to exploit the spatial association of the points to find areas where the movement is consistent and, in that way, to predict how the whole terrain mass may move during a landslide. For the clusters analyzed in this project, the PS point densities were commonly on the order of tens to hundreds of points per square kilometer.

## **A.3 RELATIONSHIP OF MEASURED DISPLACEMENT AND VELOCITIES WITH POTENTIAL SLOPE FAILURES**

The relationship between the terrain displacement or velocity, as measured with the PS InSAR technique, and the slope stability is complex. At the most basic level, a slope that shows movement will, in general, be more likely to become unstable than a slope that does not show movement—but how exactly that movement is

linked to the instability is a more difficult question to answer. We looked at certain movement characteristics, such as accelerating and decelerating trends, as these would indicate increasingly unstable or increasingly stable slope conditions, respectively, but our data, in general, did not show any of these trends in a significant way. A more sophisticated approach to the problem would be to try to model the slope stability for the areas that show movement, but this would require collecting field data and samples to assess the slope material properties, which is far beyond the scope of a general monitoring program and would be practical only at particular sites, once it has been established that they are the most critical or important (e.g., they present a direct risk for people or infrastructure).

## **A.4 EXPANDING THE TOOLS FOR FURTHER SLOPE MONITORING**

Finally, the question of how this methodology can be applied or further expanded to allow monitoring in the future was also brought up. The technology to do this kind of monitoring seems to be here to stay: in addition to the satellites we used in our study (Sentinel 1 from the European Space Agency, ESA), other agencies and countries are planning to launch their own SAR satellites and sensors. The availability of data from these sensors could contribute to making this technique more accessible and effective. Some countries, such as Norway, already have nationwide monitoring programs using this kind of method.

In terms of requirements for doing this kind of analysis, there are two main resources other than the SAR data: expertise in processing the data and computational resources. To build the expertise would require training in the processing software as well as in the fundamental knowledge of the methods theory to understand and interpret the results. The computational resources are the main processing power (e.g., a computer with enough CPU and GPU capacity) and large memory storage for the files and intermediate products (several hundred GB at least), as well as the internet bandwidth to download the data.



EUROPEAN UNION



**GFDRR**

Global Facility for Disaster Reduction and Recovery



Administered by

**THE WORLD BANK**

IBRD • IDA | WORLD BANK GROUP